



# Exploring the deformation potential of composite materials processed by incremental sheet forming: a review

Zhaobing Liu<sup>1,2,3</sup> · Kai Cheng<sup>1</sup> · Kerui Peng<sup>1</sup>

Received: 4 June 2021 / Accepted: 15 September 2021 / Published online: 2 October 2021  
© The Author(s), under exclusive licence to Springer-Verlag London Ltd., part of Springer Nature 2021

## Abstract

Over the past two decades, incremental sheet forming (ISF) has advanced the development of flexible sheet metal forming, especially for small-to-medium volume and customized production. To be suitable for various applications, researchers have explored the deformation potential of different materials, such as metals, polymers, composites, and so forth. For these materials, ISF-formed shapes and performances of the final components including formability, geometric accuracy, surface roughness, strength, and fatigue, etc. have been extensively assessed via analytical, numerical, and experimental approaches. This review article attempts to summarize the composite materials that are recognized and processed by ISF so far. Besides, deformation and failure mechanisms and constitutive equations used to describe their mechanical behaviors during ISF are discussed as well. The presented summary is aimed at aiding the ISF researchers in designing and manufacturing composite material components with desirable shapes and performances while providing a reference for future material characterizations related to sheet forming research.

**Keywords** Incremental forming · Composite materials · Properties · Deformation · Constitutive model · Formability · Roughness · Force · Accuracy · Strength

## Acronyms

ISF	Incremental sheet forming	Ti	Titanium
SPIF	Single-point incremental forming	RVE	Representative volume element
TPIF	Two-point incremental forming	PP	Polypropylene
DSIF	Double-sided incremental forming	FML	Fiber metal laminate
AISF	Asymmetric incremental sheet forming	ST	Santoprene
FSIF	Friction stir incremental forming	PVC	Polyvinyl chloride
ADSIF	Accumulative double-sided incremental forming	SiCp	Silicon carbide particles
Al	Aluminum	PMMA	Polymethyl methacrylate
Mg	Magnesium	f-MWCNTs	Functionalized multi-wall carbon nanotubes
St	Steel	PLA	Poly lactic acid
Cu	Copper or cuprum	PA	Polyamide
FGM	Functionally graded material	BFRP	Basalt fiber–reinforced thermoplastic polymer
		CFRP	Carbon fiber–reinforced plastics
		GFRP	Glass fiber–reinforced plastics
		FSTWB	Friction stir tailor welded blank
		FLD	Forming limit diagrams
		FFL	Fracture forming line
		FGBIT	Fractal geometry–based incremental toolpath
		SEM	Scanning electron microscope

✉ Zhaobing Liu  
zhaobingliu@whut.edu.cn; zhaobingliu@hotmail.com

<sup>1</sup> School of Mechanical and Electronic Engineering, Wuhan University of Technology, Wuhan 430070, China

<sup>2</sup> Hubei Digital Manufacturing Key Laboratory, Wuhan University of Technology, Wuhan 430070, China

<sup>3</sup> Institute of Advanced Materials and Manufacturing Technology, Wuhan University of Technology, Wuhan 430070, China

## 1 Introduction

Sheet metal forming has an important position in the manufacturing industry and has been widely used in the fields, such as biomedical, automotive, and transportation. ISF is a new flexible sheet metal forming technology, which does not require a specific die, and uses the generic forming tool to move along the pre-designed tool paths to form the sheet metal through a series of localized plastic deformations [1]. Compared with the traditional sheet metal forming processes, such as drawing and stamping, ISF has a short development time and low economic cost, especially suitable for small batch or customized production.

In the early stage of ISF research, it is mainly referred to as SPIF. As shown in Fig. 1, only a simple tool, usually with a small hemispherical head [2], is applied to deform the materials in the SPIF. In recent years, many variants of ISF have been proposed including TPIF with a partial or full die [3–9] and DSIF with a supporting tool [10–16]. As shown in Fig. 2, in the TPIF process, a partial or full die is added on the back of the sheet metal to increase formability and forming accuracy. For the DSIF process, the support tool is placed on the back of the sheet material as a movable supporting die with a specified trajectory.

Since Leszak [17] issued the first patent on the ISF process in 1967, the ISF technology has attracted more and more attention from academia. Some scholars have published a large number of relevant review articles. In 2003, Hagan and Jeswiet [18] described the evolution process of different incremental sheet forming techniques by comparing the traditional sheet metal forming methods (i.e., conventional spinning and shear forming) with the ISF process. Jeswiet et al. [19] introduced the types, equipment, process parameters, and applications of asymmetric incremental sheet forming in 2005. To help other researchers understand the development of ISF technology, Emmens et al. [20] introduced the development history of the ISF process.

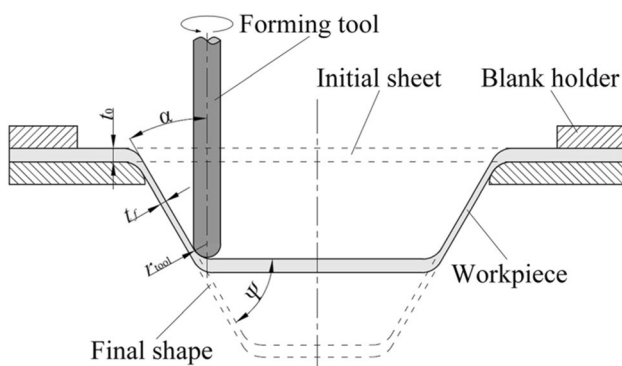


Fig. 1 The principle of the SPIF process [2]

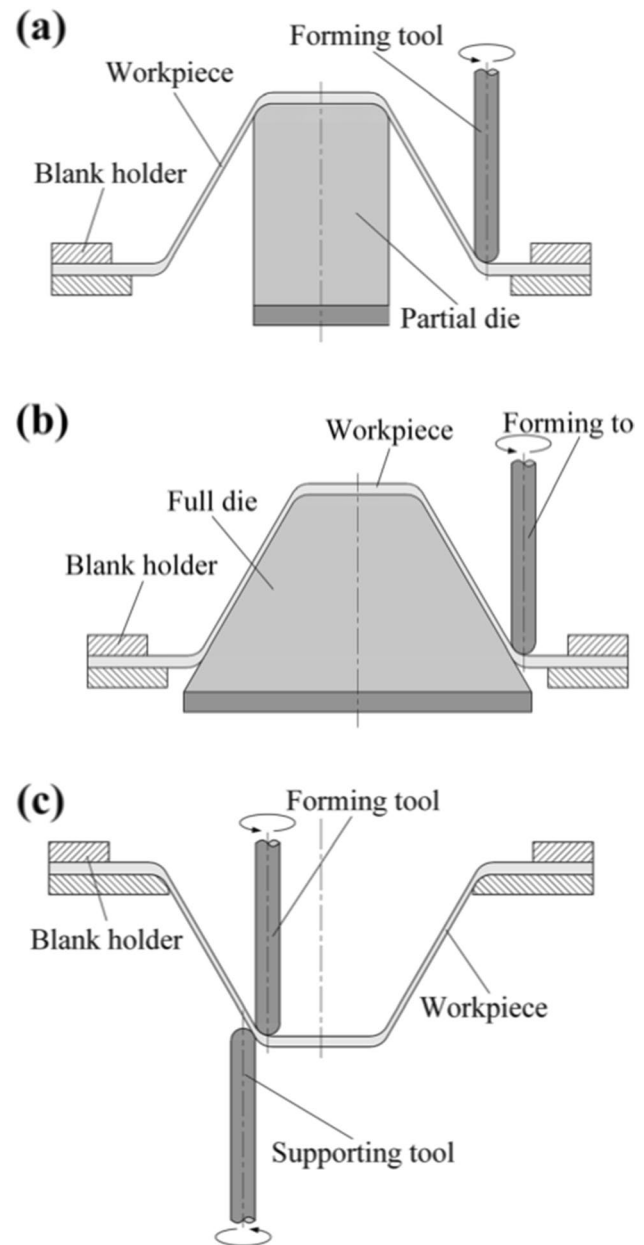


Fig. 2 The principle of different variants of the ISF process. (a) TPIF with a partial die, (b) TPIF with a full die, and (c) DSIF [2]

Behera et al. [21] reviewed the progress and the research trends of the SPIF process from 2005 to 2015. The review published by Li et al. [22] focused on the recent development of the ISF process from the aspects of deformation mechanism, modeling methods, forming force prediction, and forming quality research. Gatea et al. [23] provided a review discussing the influence of parameters on the ISF process. Lu et al. [24] presented a review that comprehensively introduced the strategies which could improve the geometric accuracy in the ISF process. The review of Ai and Long [25] is devoted to describing the possible fracture

mechanisms to explain the different failure modes. In recent years, the processing of thermoplastics using ISF technology is a hot topic in the ISF field. Zhu et al. [10] provided a comprehensive summary of the ISF process of thermoplastics. To improve formability and forming quality, many variants have been developed. The review of Liu [26] focused on the development of heat-assisted incremental sheet forming. Peng et al. [27] conducted a review for the DSIF process based on the SPIF.

Composite materials have attracted scholars' attention owing to their excellent physical and chemical properties and designability. As early as 1989, Strong and Hauwiller [28] fabricated thermoplastic composite laminate parts using the incremental forming method and compared the performance with parts of the same shape formed by matched die molding. And then in 1991, they issued a patent that was named incremental forming of thermoplastic composites [29]. Over the past few years, scholars have studied a variety of composite materials formed by the ISF, including metal composites [30], fiber-reinforced metal composites [31], polymer composites [32], and composites of metal and polymer [33]. However, to the best of authors' knowledge, there is still a lack of a detailed review that summarizes and discusses the deformation potential of composite materials by ISF. Therefore, this article provides an overview of the current status of the ISF process of composite materials to bridge this gap.

The structure of this article is as follows: following the introduction section, composite materials involved in this review are presented in Sect. 2. Section 3 reviews the process setup for composite materials. The deformation and failure mechanisms are introduced in Sect. 4. Section 5 introduces the constitutive laws and the finite element modeling for single-layer materials and composite materials. Section 6 comprehensively reviews the formability of composite materials in ISF, including formability evaluation and the effects of process parameters on formability. The reasons for studying the forming force and the effects of process parameters on forming force are discussed in Sect. 7. Then, Sect. 8 describes the forming accuracy, surface quality, strength, and fatigue in the ISF of composite materials. Section 9 has discussed the missing areas that have not been addressed so far as research directions for future work. The conclusions and research challenges about the ISF of composite materials are summarized and discussed in the final section.

## 2 Composite materials in ISF

In this review, we first discuss the composite materials that have already been used in the ISF process, which mainly include metal composite materials, composites of metal and

polymer, fiber-reinforced composite materials, and other composite materials.

### 2.1 Metal composites

The multi-metal composite sheets have an extensive range of applications in automotive, electrical, energy storage, and heat transfer because of the combined mechanical, physical, and chemical properties of different substrates [34–36]. In recent years, the SPIF of metal sheets has received the attention of many researchers. Neugebauer et al. [30] applied the incremental forming method to study the contact and forming conditions of Al–Mg composite sheets by finite element simulation. The Ref [37] referred to the study of the forming of Al–St composite sheets using AISF. The results displayed that the formability of composite material is lower than that of the two substrates. Abd Ali et al. [38, 39] investigated the effects of process parameters on the formability, failure modes, and surface roughness of Al–St composite sheets. Ghassabi et al. [40] analyzed the effects of process parameters such as step size, feed speed, movement strategy, and spindle speed on the accuracy, forming force, thickness distribution, and failure modes in the welding zone of Al–St composite sheets. Wu et al. [41, 42] numerically and experimentally analyzed the friction stir–assisted incremental forming with synchronous bonding of Al–St composite sheets. Liu and Li [43] studied the effects of various parameters on the formability, surface finish, thickness variation, and forming force of Cu–Al composite sheets by analytical, empirical, and numerical methods. The results displayed that the Al/Cu layer arrangement (Al/Cu layer arrangement is referred to the bilayer sheet in which the Al layer is in contact with the forming tool) has higher formability and larger forming force compared with the Cu/Al layer arrangement. Gheysarian and Honarpisheh [44, 45], Honarpisheh et al. [46, 47], and Qin et al. [48] carried out mathematical, numerical, and experimental studies on the SPIF of Cu–Al composite sheets. Alinaghian et al. [49] focused on the study of effects of parameters including spindle speed, step size, and tool diameter on the residual stress of Al–Cu composite sheets by using the incremental hole-drilling method. Bouhamed et al. [50] first used homogenization of elasto-plastic FGM based on the representative volume element to simulate the deformation behavior of Al–Ti composite sheets in the SPIF process. The Mori–Tanaka model and RVE were used to estimate the elastic effective properties of FGM composites. Sakhtemanian et al. [51–53] experimentally and numerically analyzed the effects of parameters and ultrasonic vibration on SPIF process of St–Ti composite sheets. Hassan et al. [54, 55] investigated the formability and delamination of St–St composite sheets in the SPIF process. Ashouri and Shahrajabian [56] studied the effects of layer arrangement, step size, tool radius, and feed speed on the

formability of Brass–St13 composite sheets in the SPIF process. Wei et al. [57] proposed a combination of parameters that had a controlling effect on the interior surface roughness. Al1060 sheets and Cu–St composite sheets were used to verify this combination. Al-Ghamdi and Hussain [58–63] studied the effects of annealing temperature, tool diameter, feed speed, step size, and spindle speed on the formability, bulging defect, surface roughness, and residual stress-gradient of Cu–St–Cu composite sheets in ISF. Shi et al. [64] experimentally studied the residual stress states of Cu–St–Cu composite sheets formed by the SPIF with the hole drill method. The results indicated that the wall angle and tool diameter had the greatest effect on the residual stress, while the spindle speed had the least effect on the residual stress. The parameter combination of small diameter, large wall angle, high feed rate, medium step size and spindle speed, and material rolling conditions (i.e., no annealing) resulted in high residual stress. Wei and Hussain [65] experimentally studied the effect of the ISF process parameters on the tensile properties of Cu–St–Cu composite sheets. They found the deformation angle and annealing temperature were the most important parameters affecting the tensile properties after the ISF deformation. In addition to formability and failure behavior, the economic costs and energy consumption in the ISF of the metallic composite materials were also considered in some papers. Hussain and Al-Ghamdi [66] systematically analyzed the indicators including energy, cost, and productivity as functions of ISF parameters of Cu–St–Cu composites. They concluded that high step size and feed rate values, low wall angles, spindle speed, and annealing temperature values should be used to reduce costs and energy requirements while increasing productivity. In another work, to characterize the carbon dioxide emissions during the ISF of the Cu–St–Cu composite sheet, Al-Ghamdi and Hussain [67] presented a forecast model of carbon dioxide emissions and environmental costs.

## 2.2 Fiber-reinforced composites

Fiber-reinforced composite materials, especially CFRP and GFRP, are widely used in aircraft, marine, automotive, civil, and biomedical fields owing to their excellent properties, such as low specific gravity, high specific strength, and excellent corrosion resistance [68–73]. Conte et al. [74], Ambrogio et al. [75], and Al-Obaidi et al. [76] performed the studies on the heat-assisted SPIF of glass fiber–reinforced PA6 composite sheets. Hou et al. [77] developed a heat-assisted SPIF method for jute fabric–reinforced PLA composite sheets. They also analyzed the effects of clamping mode, tool path, step size, and thickness on the formability of composites. Torres et al. [78] designed hot water–assisted SPIF process to form linen fiber–reinforced Solanyl composite sheets. And the effects of step size, forming temperature,

and wall angle on the formability of composite plates were studied. Okada et al. [79] developed an incremental forming method for carbon fiber–reinforced PA6 composite sheets using a halogen lamp heating system. Simple spot-forming was used to evaluate the fundamental forming characteristics of the developed system. They evaluated the advantages of the developed method by using two-dimensional sheet-fed forming to obtain the shape profile of the formed product. Xiao et al. [80] numerically and experimentally investigated the ISF process of CFRP composite sheets. The results indicated that it is possible to apply the ISF process to deform CFRP composite sheets with single or multilayer prepregs.

## 2.3 Composites of metal and polymer

The composites of metal and polymer are relatively common composite materials, and their forming force, formability, and failure behavior have attracted scholars' attention. Galdos et al. [33] conducted a study on the formability, forming force, and failure behaviors of St–Polymer–St composite sheets. According to the study of Harhash and Palkowski [81], the possibility of SPIF for St–Polymer–St sandwich composite sheets was investigated. The results have shown that the fracture of composite sheets occurs earlier than that of steel sheets in ISF. In the study of Jackson et al. [82], results have revealed that the St–PP–St and Al–PP–Al sandwich panels have similar forming force trends, through-thickness deformation, and accuracy. A geometric model, sine law, could be also used to predict material thinning after the ISF. Girjob and Racz [83] formed the Al–PP–Al composite sheets by the SPIF process. The preliminary results have shown that the suitable process parameters (such as feed speed, tool diameter, and spindle speed) and process trajectory can produce satisfactory parts. Liu and Chen [84] investigated the deformation behaviors and failure-tolerant characteristics of Al–PA composite sheets under different loading conditions. Their results indicated that four failure modes could be identified, including one-layer fracture, two-layer fracture, delamination, and their mixed case in the ISF process. Davarpanah and Malhotra [85] investigated the effects of metal thickness, polymer thickness, and step size on the formability and failure mode of metal–polymer composite plates during the SPIF process. They concluded that the higher polymer thickness led to the higher formability, and the failure mode depended on the metal thickness and the polymer thickness.

## 2.4 Other composites

Given the current literature, the manufacture of some special composite material components by the ISF process is also promising. Walczyk et al. [86] manufactured the composite aircraft parts using reconfigurable tooling and surface



heating with the ISF. They demonstrated that this novel composite forming method could successfully produce composite parts without dimples and wrinkles. Fiorotto et al. [31] formed the FMLs using the SPIF process. First, they assessed the possibility of rapidly and economically forming molds with complex geometric shapes made of aluminum. Then, the experiments of direct incremental forming of the FMLs were carried out. Different types of diaphragms made of aluminum and PVC were used to avoid the failure mode namely wrinkling and accelerate the adhesion of the composite. The results indicated that the specific stiffness and strength of composite laminates formed by SPIF were significantly improved. AL-Obaidi et al. [87] used the SPIF process supported by hot air heating to form FMLs into the desired shape. The results showed that a wall angle that was greater than or equal to  $50^\circ$  produced delamination and voids. Hernández-Ávila et al. [32] experimentally studied the SPIF process of PP-ST composite sheets. Through the characterization of the mechanical properties and fracture mechanism of 6092Al-SiCp composites (AMC), Gatea et al. [88] studied the feasibility of forming 6092Al-SiCp composite sheets by the ISF process under the different heat treatment conditions. The results indicated that the composite sheets had the best formability under the heat treatment condition of O-condition annealing, and the formability improved with the low feed speed. Clavijo-Chaparro et al. [89] developed a composite material that was composed of PMMA used as base material, triacetin used as a plasticizer, and Cloisite 30B used as reinforcement. The experimental results of the SPIF revealed that the mechanical interlocking effect between the Cloisite 30B and the PMMA chain could enhance the formability of the composites. In contrast, the results of Jackson et al. [82] have revealed that St-St fiber-St and Al-Al foam-Al could not be formed by the ISF. Boric et al. [90] studied the preparation and characterization of polymer materials including a mixture of neat PA12, a nanocomposite with PA12 matrix and 1% Cloisite 93A, and a nanocomposite with PA12 matrix and 3% Cloisite 93A, which were suitable for the SPIF process. Matsumoto et al. [91] applied the FSIF process to connect commercial molded nickel foams with PMMA sheets for manufacturing the porous metal–nonporous resin composite. The results showed that the joining strength between the foam and the sheet material exceeded the fracture strength of the foam. They also concluded that the sheet was mechanically interlocked (anchored) to the porous structure of the foam by the plastic flow of the heated and softened PMMA into the surface pores of the foam. Lozano-Sánchez et al. [92] fabricated the PP-MWCNTs composite sheets using the SPIF process. They concluded that the mechanical strength of the polymer matrix is enhanced by the presence of small quantities ( $< 1$  wt%) of f-MWCNTs without affecting the formability of the polymer matrix.

## 2.5 Summary

The composite materials involved in this review article are classified and summarized in Table 1.

## 3 Process setup for composite materials

### 3.1 Conventional ISF setup

The ISF setup for the composite materials is similar to that of the single-layer metal sheets which are composed of the positioning system, forming tool, clamping fixture, and support structure [94]. Liu and Li [43], Abd Ali et al. [38], and Sakhtemanian [51] used a milling machine with an experimental setup for the ISF of Al-St, Cu-Al, St-Ti composite sheets. The equipment consists of the composite sheet blank, the blank holder, the backing plate with a hole, and the forming tool. Hernández et al. [32] and Lozano-Sánchez et al. [92] equipped a machining center to perform the SPIF experiments to shape the PP-ST composite sheet and PP-MWCNTs composite sheet.

### 3.2 Specific ISF setup

For many metal composites, ISF is possible at room temperatures. However, for some composite materials that are difficult to deform at room temperatures, especially fiber-reinforced composites, a special setup is needed to assist the ISF process.

#### 3.2.1 Heat-assisted ISF setup

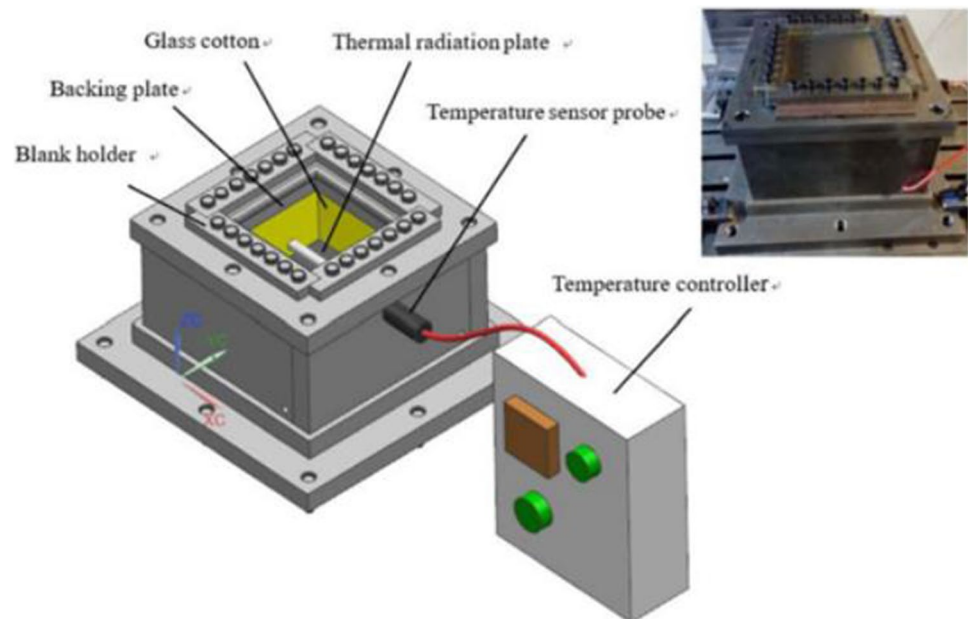
Some researchers have developed different heating methods to heat composite sheets to make them easier to deform. In this section, the ISF heating setups are classified and discussed according to the different types of heat sources.

**Heat from thermal radiation** When forming the jute fabric-reinforced PLA composite sheet, Hou et al. [77] used a thermal radiation plate to heat the sheet, as shown in Fig. 3. To store heat, the hollow space inside the fixture was equipped with glass cotton. The heat generated by the heat radiation plate was regulated by a temperature controller with a temperature sensor probe.

**Heat from resistor** To form a composite sheet that was made of PA6 and short glass fibers, Ambrogio et al. [74, 75] installed a 2-kW resistor to heat the air, which could transfer the heat to the composite plate in a thermal isolation chamber without much heat loss. The heating temperature

**Table 1** The composite materials involved in this article

Material type	Materials	References
Metal composites	Al-St	[37–42, 93]
	Al-Cu	[43–49]
	Al-Mg	[30]
	Al-Ti	[50]
	Cu-St	[57]
	Cu-St-Cu	[58–67]
	St-Ti	[51–53]
	St-St	[54, 55]
	St-Brass	[56]
Fiber-reinforced composites	Jute fabric-reinforced PLA	[77]
	Carbon fiber-reinforced PA6	[79]
	Glass fiber-reinforced PA6	[74–76]
	Linen fiber-reinforced Solanyl	[78]
	Carbon Fiber-reinforced Epoxy Resin	[80]
Composites of metal and polymer	St-Polymer-St	[33, 81]
	St-PP-St	[82]
	Al-PP-Al	[82, 83]
	PA-Al	[84, 85]
Other composites	PP-ST	[32]
	Fiber-reinforced Metal Composites	[31, 87]
	Nickel Foam-PMMA	[91]
	Plasticized and Reinforced PMMA	[89]
	PP-MWCNTs	[92]
	Al-SiCp	[88]
	St-St Fiber-St	[82]
	Al-Al Foam-Al	[82]
PA-Cloisite 93A	[90]	

**Fig. 3** The ISF setup with thermal radiation plate heating [77]

was controlled by an external control unit connected to the resistor. The details of this SPIF equipment are presented in Fig. 4.

**Heat from hot air** In the research of AL-Obaidi et al. [76, 87], as shown in Fig. 5, a hot air pump heating device placed next to the holding fixture was used to heat the glass

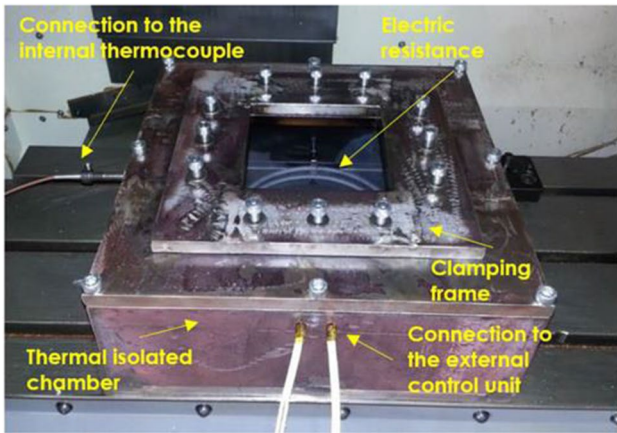


Fig. 4 The resistor heat-assisted setup [75]

fabric and aluminum sheets during the ISF. The heating device consists of resistance heaters with an air pump that was piped to deliver hot air to an insulated hot chamber located inside the fixture. The insulated hot chamber is made of silicate material to reduce heat loss between the internal laminate and the external environment. Furthermore, the heating temperature was controlled by an analog converter device connected with the thermocouples.

**Heat from a halogen lamp** As shown in Fig. 6, Okada et al. [79] developed an optical heating system consisting of a halogen lamp. The halogen lamp was placed on one side of the carbon fiber–reinforced PA6 composite sheet to achieve local heating. A reciprocating spherical forming punch can form the heating area of the workpiece on the other side of the sheet.

fiber–reinforced thermoplastic polymer (PA6GF47) composite sheets and BFRP laminates consisting of basalt fiber

**Heat from hot water** According to the study of Torres et al. [78], the hot water–assisted ISF setup was developed to

Fig. 5 The ISF setup with a hot air pump [76]

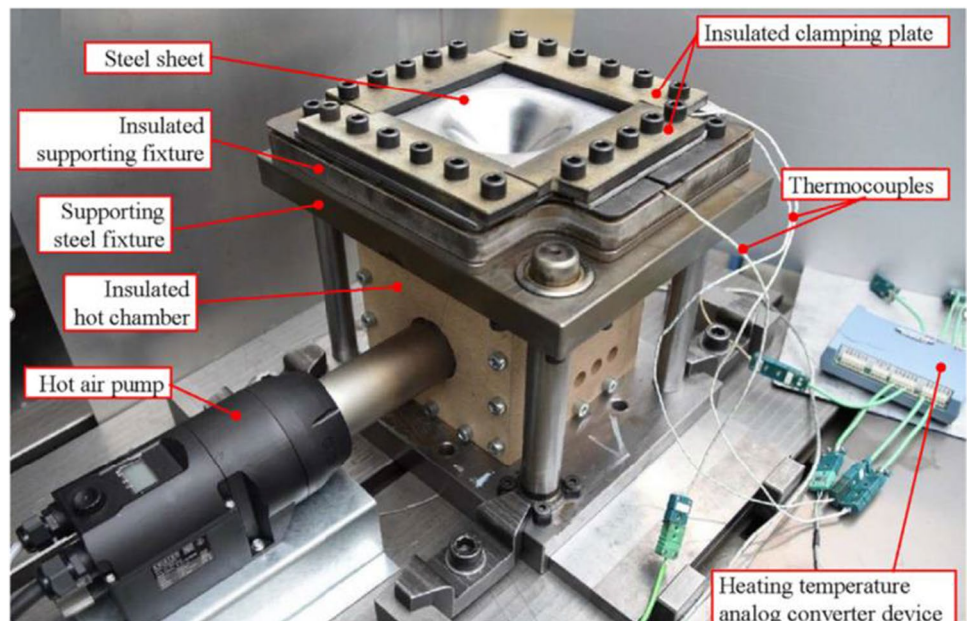
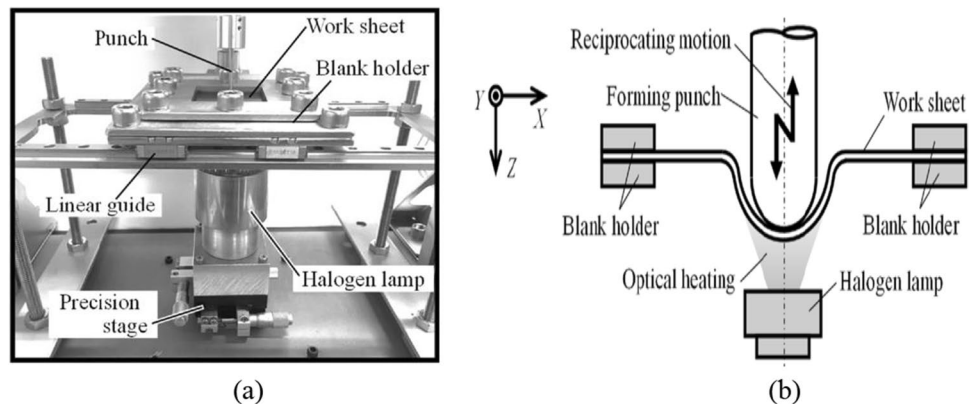
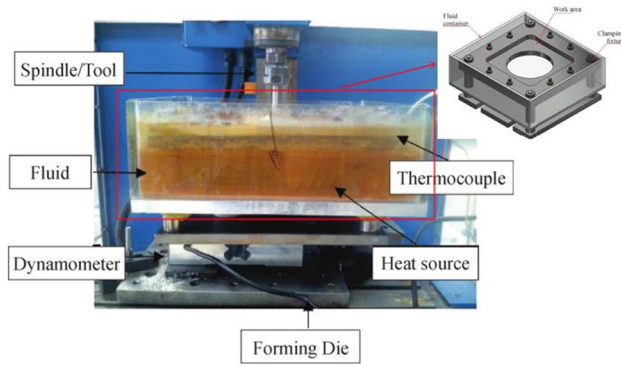


Fig. 6 (a) Experimental setup using a halogen lamp and (b) schematic illustration of the process operation [79]







**Fig. 7** The hot water–assisted heating setup [78]

globally heat the linen fiber–reinforced Solanyl composite sheets. As shown in Fig. 7, the composite sheet and clamping fixture are completely immersed in the water medium and the temperature of the water medium could be regulated by the external control unit with a thermocouple.

**Heat from friction** When the friction heat is sufficient to soften the composites, the heating device may not need to be used. Li et al. [42] utilized a spindle speed of 3000–6000 rpm to form and bond the aluminum alloy and steel

laminated metal sheets. In the study of Matsumoto et al. [91], the PMMA sheet was joined with the open-cell nickel foam under the FSIF conditions with the rotation rate faster than 2000 rpm and the feed rate slower than 60 mm/min.

### 3.2.2 Ultrasonic-assisted ISF setup

For some metal composites which are difficult to be formed at room temperatures, the SPIF assisted by the ultrasonic vibration is also a good choice. In the study of Sakhtemanian et al. [53], ultrasonic vibration devices were used during the SPIF process of the St-Ti composite sheet, as shown in Fig. 8. The system includes an ultrasonic generator and a longitudinal transducer. An ultrasonic generator with a power of 2 KW and a frequency of 20 kHz plays a role in converting the frequency of 50–60 Hz current to the high frequency (20 kHz) current. Longitudinal transducers can convert the electrical energy into mechanical vibrations with longitudinal modes. Then, the vibration could be transmitted to the tool holder and further be amplified by the attached vibration tool.

**Fig. 8** The ultrasonic-assisted ISF setup [53]

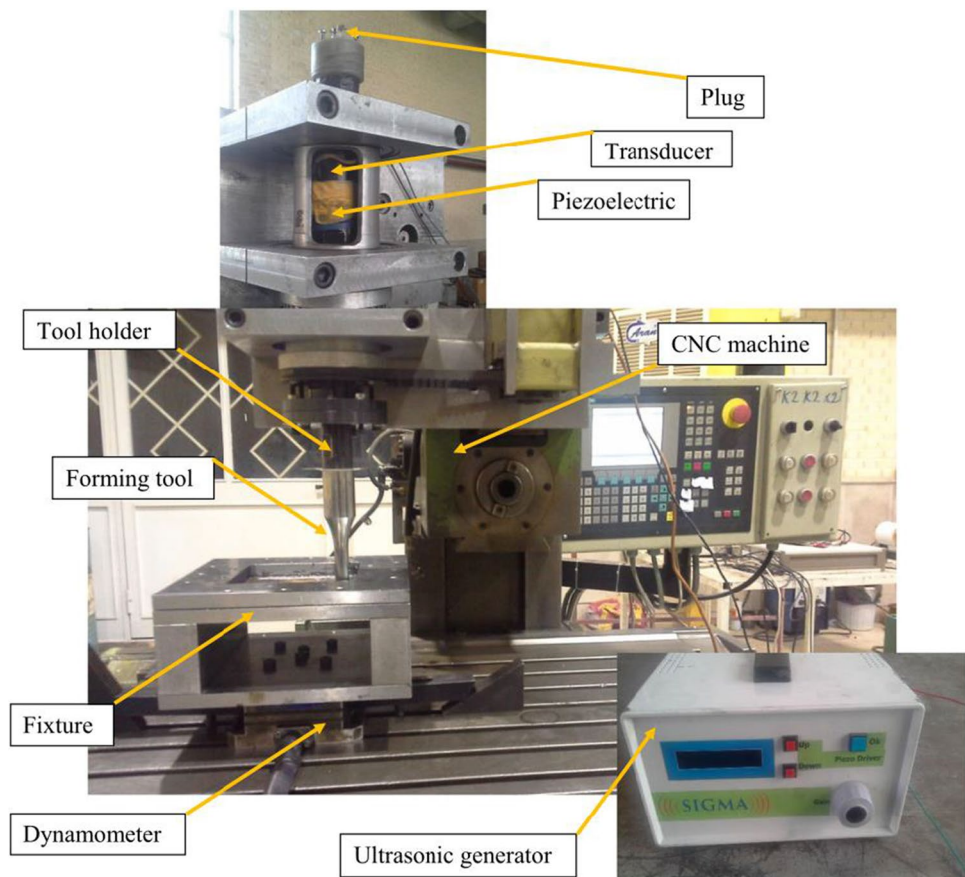




**Table 2** The summary of specific ISF methods

Methods	Research	Materials	Advantages	Disadvantages
Thermal radiation plate heat	Hou et al. [77]	Jute fabric–reinforced PLA	Easily controlled temperature	Complex the heating and heat preservation devices
Resistor heat	Ambrogio et al. [74, 75]	Glass fiber–reinforced PA6	Easily controlled temperature	Complex the heating and heat preservation devices
Hot air heat	AL-Obaidi et al. [76, 87]	Glass fiber–reinforced PA6 and BFRP laminates	Uniform heating and easily controlled temperature	High hardware cost
Halogen lamp heat	Okada et al. [79]	Carbon Fiber-reinforced PA6	Simple operation	Slow heating rate and uneven heating
Hot water heat	Torres et al. [78]	Linen Fiber reinforced Solanyl	Uniform heating and easily controlled temperature	Low forming temperature (up to 100 °C)
Friction heat	Li et al. [42] and Matsu-moto et al. [91]	Al-St and Nickel Foam-PMMA	No additional equipment	Low forming temperature; severe tool wear and poor surface quality of parts
Ultrasonic-assisted forming	Sakhtemanian et al. [53]	St-Ti	Rapid increase in tool temperature due to ultrasonic vibration	Complex devices

**3.2.3 Summary**

The pros and cons of the specific ISF setup are summarized and discussed in Table 2.

$$d\sigma_\theta = -\mu_\theta \sigma_t \frac{rd\theta}{t} \cong -\mu_\theta \sigma_t \tag{1}$$

$$\frac{\sigma_t}{t} + \frac{\sigma_\varnothing}{r_1} + \frac{\sigma_\theta}{r_z} = 0 \tag{2}$$

**4 Deformation and failure mechanisms**

**4.1 Deformation mechanism**

The main deformation mode in ISF of metal composite sheets is the membrane strain caused by stretching [95–97]. The study on other deformation mechanisms including shear deformation and bending under tension that are applied in the analysis of ISF processing composites has not been found.

**4.1.1 Membrane strain**

Some researchers propose that the main deformation mode during the ISF process is stretching leading to membrane strain. As shown in Fig. 9, Silva et al. [97] divided the possible forming paths into three basic deformation modes: (a) flat surfaces under plane strain stretching mode, (b) rotationally symmetric surfaces under plane strain stretching mode, and (c) corners under equal biaxial stretching mode. Silva et al. [96] analyzed the membrane equilibrium conditions of the local shell element, as shown in Fig. 10. The simplified membrane analysis equilibrium equations along with the circumference, meridian, and thickness directions are shown as follows:

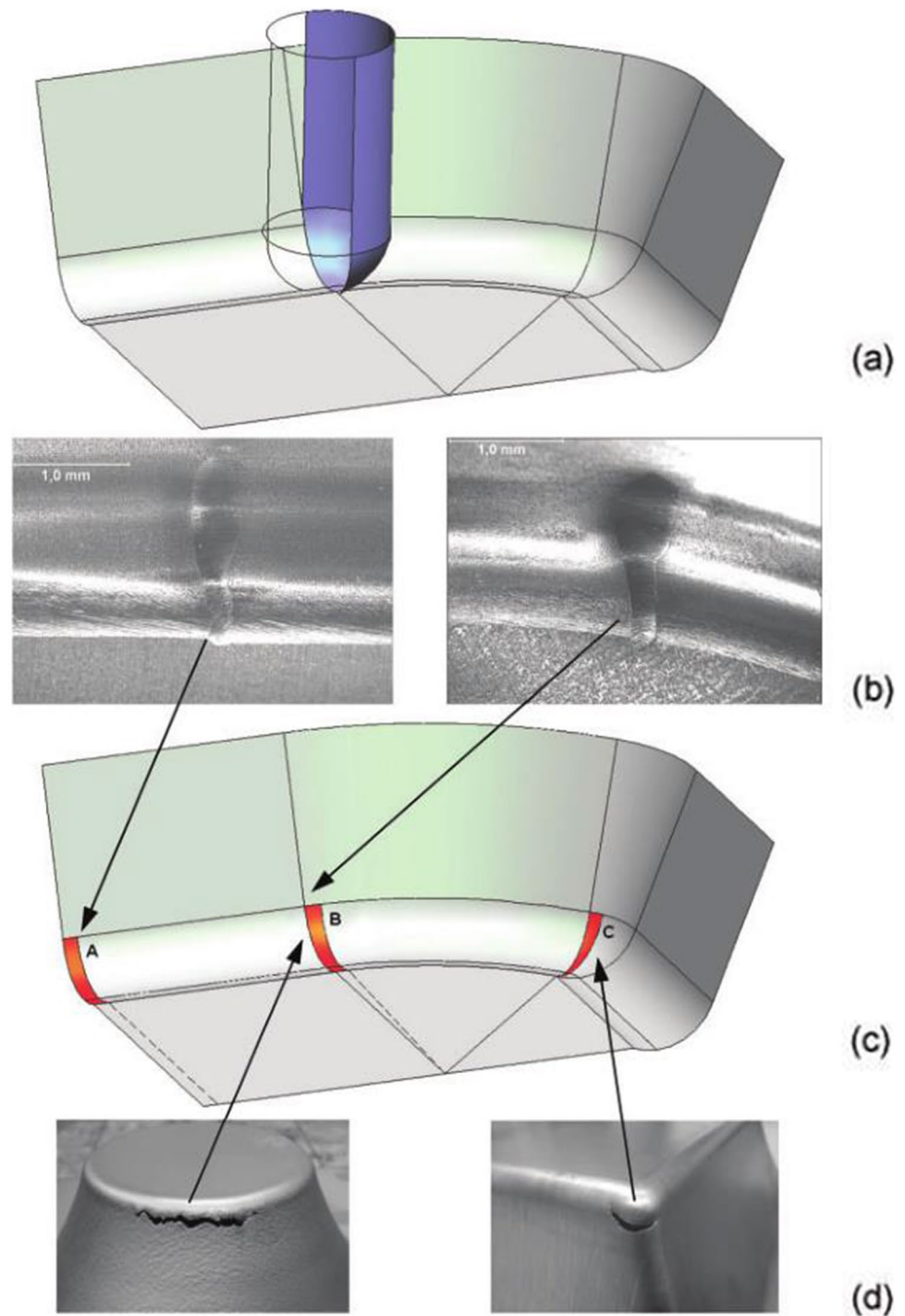
$$\frac{d\sigma_\varnothing}{dr} + \frac{\sigma_\varnothing - \sigma_\theta}{r} + \frac{\mu_\varnothing \sigma_t}{t \sin\alpha} + \frac{\sigma_\varnothing}{t} \frac{dt}{dr} = 0 \tag{3}$$

where  $\sigma_\theta$ ,  $\sigma_\varnothing$ , and  $\sigma_t$  represent the circumferential stress, meridian stress, and thickness stress respectively;  $\mu$  is the friction coefficient;  $t$  is the sheet thickness;  $r_1$  is the curvature radius of the meridian at the element ( $r_1 = r_{tool}$ );  $r_z$  is the element normal radius where it cuts the  $z$ -axis.

**4.1.2 Shear deformation**

The experimental results for single-layer metal materials indicate that the through-thickness shear exists in the ISF process, which may be one of the main reasons for the increase of formability. The study of Allwood et al. [98] demonstrated that the through-thickness shear exists in the ISF process. And then, Jackson and Allwood [99] investigated the strain distribution through the thickness along the cross-sectional plane of the parts formed by the SPIF and TPIF processes. The experimental results revealed that for both SPIF and TPIF processes, the deformation mechanisms were stretching and shear in the radial–axial plane which was perpendicular to the tool direction as well as shear in the tool direction. Malhotra et al. [100] applied finite element simulation model to forecast the fracture of parts. They concluded that through-thickness shear and local bending of the sheet around the tool greatly affects the fracture in SPIF.

**Fig. 9** Schematic illustration of the volume element, and the basic deformation modes in SPIF: (a) flat surface under plane strain stretching mode; (b) rotationally symmetric surface under plane strain stretching mode; (c) corner under biaxial stretching mode. Note: the insets show pictures of typical cracks that occur in deformation modes (b) and (c) [97]



Smith et al. [101] investigated the difference of deformation mechanism between SPIF and ADSIF by numerical simulation. They found that the parts formed by the ADSIF process were affected by greater hydrostatic pressure, greater plastic strains and through-thickness shear strains than those formed by SPIF, which may be the reason for the improved formability of ADSIF. In the study of Lu et al. [102], the effects of friction-induced through-thickness shear were discussed.

The results showed that the effect of higher shear stress is to improve the deformation stability and stress triaxiality, but to reduce the formability.

#### 4.1.3 Bending under tension

Some researchers suggested that the bending under tension was also a deformation mode in ISF of single-layer

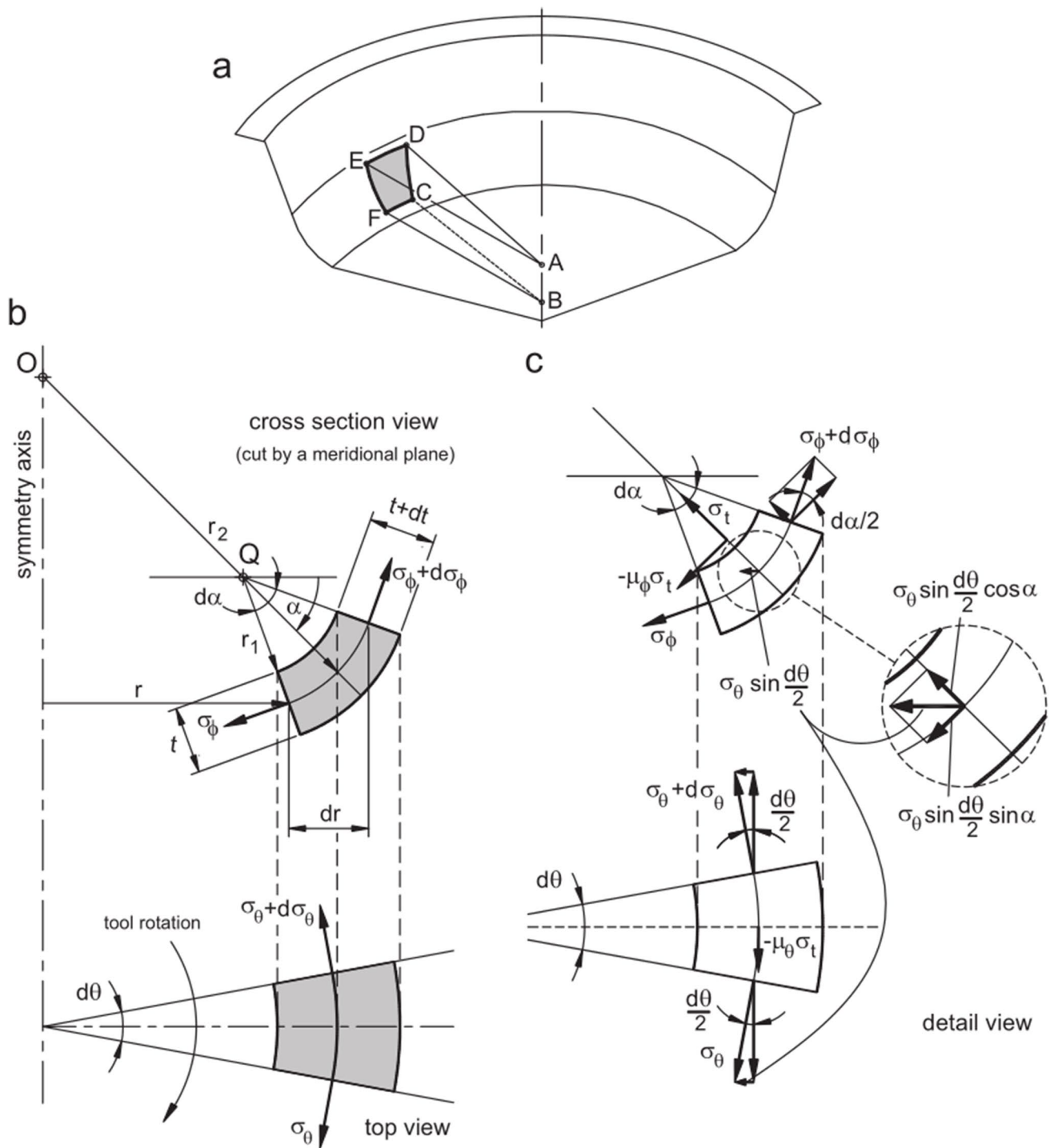


**Fig. 10** Rotational symmetric SPIF process: (a) illustration of the shell element in perspective; (b) illustration of the shell element after being cut by an axial meridional plane and as it is seen from the top; (c) details of (b) showing the acting stresses [96]

metal materials. Emmens and Boogaard [103] performed tension tests with repetitive bending to simulate a deformation pattern in the ISF process called bending under tension. They concluded that a slight bending was enough to cause great uniform strains of the sheets. In a review [104],

they describe the important role of the deformation mode of bending under tension in the ISF process. And they proposed that the occurrence of bending under tension in the ISF process was difficult to determine directly. And the tensile force was affected by both tensile and bending strains. Fang et al.

[105] described the localized deformation mechanism in the SPIF process considering both strain hardening and bending effect. The results indicated that the deformation occurs in the contact area and the wall near the contact area. Furthermore, fractures were more likely to occur at the transition area between the contact area and the formed wall.

The bending under tension was also mentioned in the ISF of composite materials. In the research of Al-Ghamdi and Hussain [62], the analysis of bending under tension revealed that the bulge was the result of bending moment applied to sheet metal by the forming tool during the ISF process. In addition, with the increase of bending moment, the height of the bulge structure increases linearly.

## 4.2 Failure mechanisms

The failure behaviors of metallic materials have been extensively investigated and reviewed, but there is still a lack of overview to summarize failure mechanisms of composite materials formed by ISF. In this section, the failure types of various composite materials are introduced and discussed.

## 4.3 Failure analysis of metal composite materials

Different from monolithic sheets, the possible failure modes of bonded multilayer metal composites by SPIF are more complicated. According to the literature review, the three modes were identified as follows:

Mode 1: Fracture without delamination, as shown in Fig. 11.

Mode 2: Fracture with delamination, as shown in Fig. 12b.

Mode 3: The bulge defect, as shown in Fig. 13.

In Abd Ali et al. [38], regardless of the Al/St layer arrangement or the St/Al layer arrangement, the fracture started from the stiffer and thinner St layer because the area of the St layer decreased less than that of the Al layer. Compared with the St/Al layer arrangement, the fracture in the Al/St layer arrangement occurred earlier because the thinner and lower ductility St layer located on the outer side of the Al/St layer arrangement underwent greater stretching deformation. Furthermore, the authors found that the delamination occurred only in the St/Al layer arrangement, as shown in Fig. 12b. It was concluded that the delamination occurred after the fracture. Liu and Li [43] found that different layer arrangements of Cu-Al composite sheets had different failure behaviors. For the Al/Cu layer arrangement, cracks appear first in the Cu layer and then in the Al layer, which was due to the thin but strong Cu layer in the outer layer withstood more stretching deformation, thereby delaying the fracture occurrence of the composite sheet. However, in the Cu/Al layer arrangement, the crack was simultaneously observed in both the Cu layer and Al layer because the bonding strength between the two layers was strong. Hassan et al. [54] performed the delamination analysis in the SPIF of the steel/steel composite sheet. The authors found no delamination of the materials at a depth of 7 mm which was the maximum forming depth in their experiments. Then, they performed finite element simulations and revealed that if the material formability was high enough, then the delamination would occur at a depth of 8.4 mm. In another paper [55], they showed that the failure mode of steel–steel composite sheets prepared at different

**Fig. 11** The failure mode of fracture without delamination for Al/Cu layer arrangement [43]

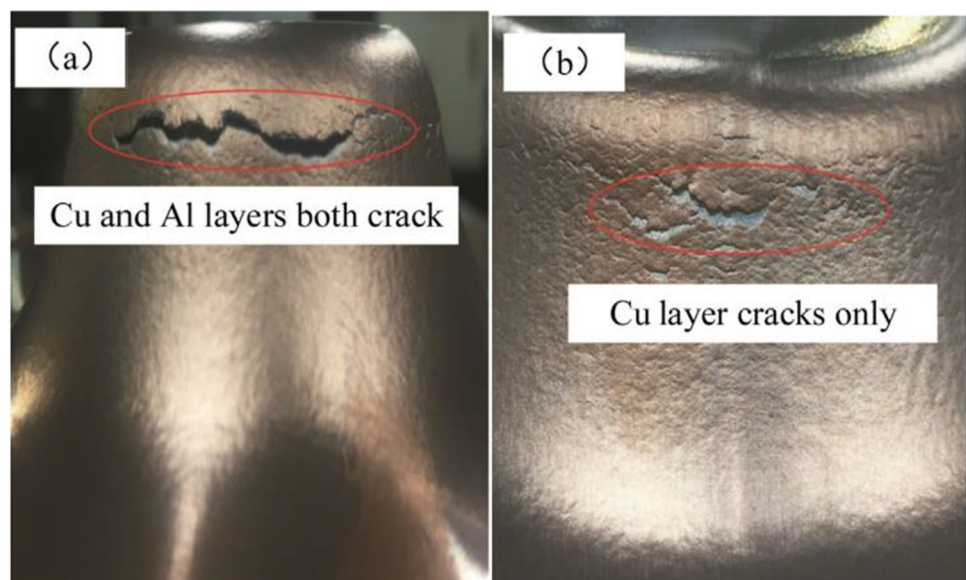




**Fig. 12** Interface morphology of composite sheets. (a) The Al/St fractured part, (b) the St/Al fractured part, and (c) the St/Al successful part [38]

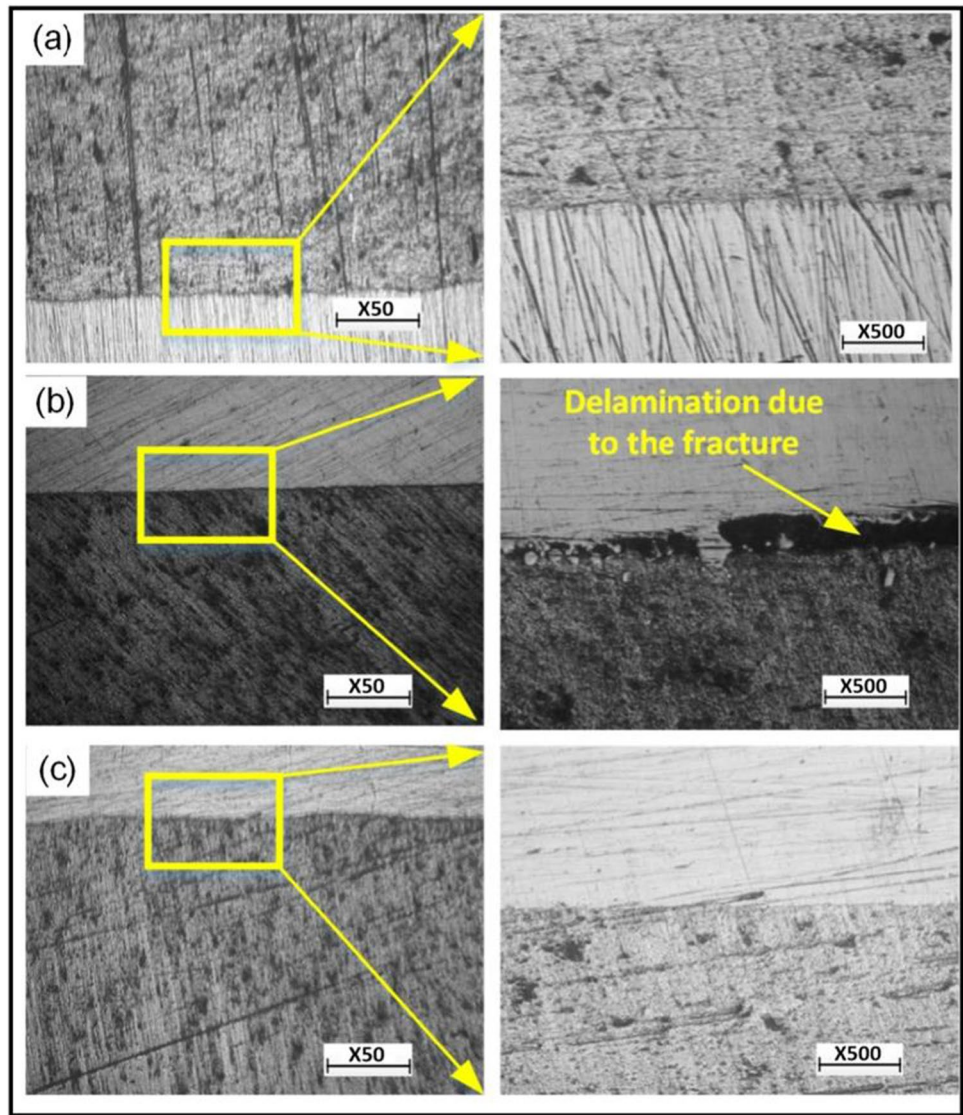


**Fig. 13** The failure mode of the bulge defect. (a) Schematic of bulge defect and (b) bulge defect in actual part [48]



pre-rolling temperatures is two-layer fracture rather than delamination. The bulge structure is also considered a failure mode because it causes faster tool wear and geometric inaccuracy. AL-Ghamdi and Hussain [62] investigated the influence of forming conditions and bending on the bulge in the ISF of Cu-St-Cu composite sheet. The results have shown that the use of high step size, large tool diameter, and moderate annealing temperature was beneficial to reduce the

height of the bulge. Furthermore, the analysis of bending under tension has shown that the height of the bulge was the result of the bending moment exerted on the sheet by the forming tool during the ISF process. Moreover, the height of the bulge could decrease by reducing the bending moment. In the research of Li et al. [42], the layer arrangement was the most important factor influencing the height of bulge, and the height of bulge for the Al/St layer arrangement was

larger than that of the St/Al layer arrangement because the material flow of AA5052 was easier than DC05 at elevated temperatures. In addition, larger spindle speed also resulted in the greater height of bulge, which could be explained that more friction heat caused the material to flow more severely and then led to the higher bulge structure. In the study of Qin et al. [48], the bulge defect is caused by the inconsistency of stress states on the upper and lower surfaces of the composite sheet. They concluded that the most important factor affecting the height of the bulge structure was step size. With the increase of step size, the height of the bulge structure also increased. Tool diameter and the coefficient of friction between the tool and the composite sheet also affected the height of the bulge structure. Large tool diameter and coefficient of friction reduced the height of the bulge structure.

#### 4.4 Failure analysis of fiber-reinforced composite materials

For the fiber-reinforced composite materials, the modes of possible failure by SPIF could be summarized as follows:

Mode 1: Circumferential cracks (see Fig. 3(b) in Hou et al. [77])

Mode 2: Oblique cracks (see Fig. 3(c) in Hou et al. [77])

Mode 3: Wrinkle, as shown in Fig. 14

Mode 4: Void, as shown in Fig. 16

According to Hou et al. [77], the stretching mechanisms due to meridional tensile stresses led to the circumferential crack, which was similar to the in-plane fracture mechanism of the PVC sheet [106] and the metal sheet [97]. The oblique crack might be related to the debonding at the interface of

the composites because the fibers elongate significantly. When the forming angle of pyramidal parts was greater than  $60^\circ$ , Xiao et al. [80] found that the wrinkle was more likely to appear at the wall area and corner, as shown in Fig. 14. In the study of AL-Obaidi et al. [76], the largest cracks in the samples occurred in the walls with wall angles of  $50^\circ$  and  $55^\circ$ , which was due to the increase in the displacement increasing the tensile fabric fibers. As shown in Fig. 15 a and b, no completely longitudinal cracks were observed, but the cracks grew longitudinally, while the fiberglass did not fracture at all. It could be seen that cracks were caused by the excessive elongation and delamination between woven fibers in Fig. 15c. The crack voids were triggered by the growth of small cracks which were observed at the boundaries of the glass fibers as illustrated in Fig. 16. However, the air voids occurred during heating and gradual cooling.

#### 4.5 Failure analysis of composites of metal and polymer

In the study of Liu and Chen [84], the failure modes of PA-Al composite sheets were very complex, including fractures of single layer, two layers, delamination, and the mixed situation. Figures 17 and 18 show the failure modes of PA-Al laminates under the 2D groove deformation path and the 3D trunk-cone deformation path respectively. The authors found that the various degrees of delamination between the Al layer and PA layer could be seen in all the experimental cases, which was mainly due to the weak adhesion between the Al layer and PA layer. Only the cracking of Al layer with no visible delamination could be observed in Fig. 18 a and b, which indicated that the composite sheet has undergone synergistic deformation and could further improve its

**Fig. 14** The wrinkle in the wall area and corner of a CFRP pyramidal part [80]

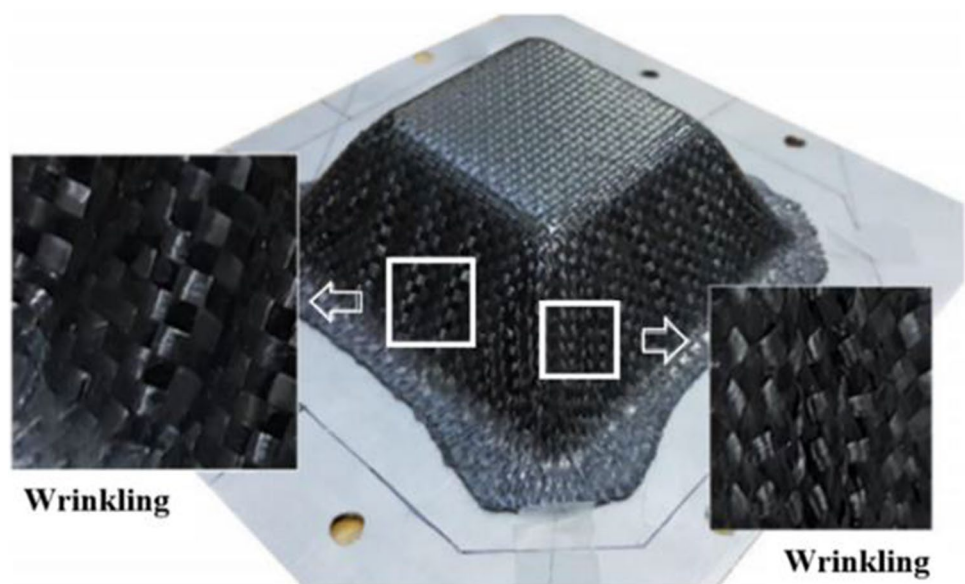


**Fig. 15** SEM examination of cracks in 55° wall angle sample: (a) detected by a high-definition backscattered electron detector, (b) enlarged view from (a), (c) was scanned by the second detector of topographic contrast, and (d) enlarged view from (c) [76]

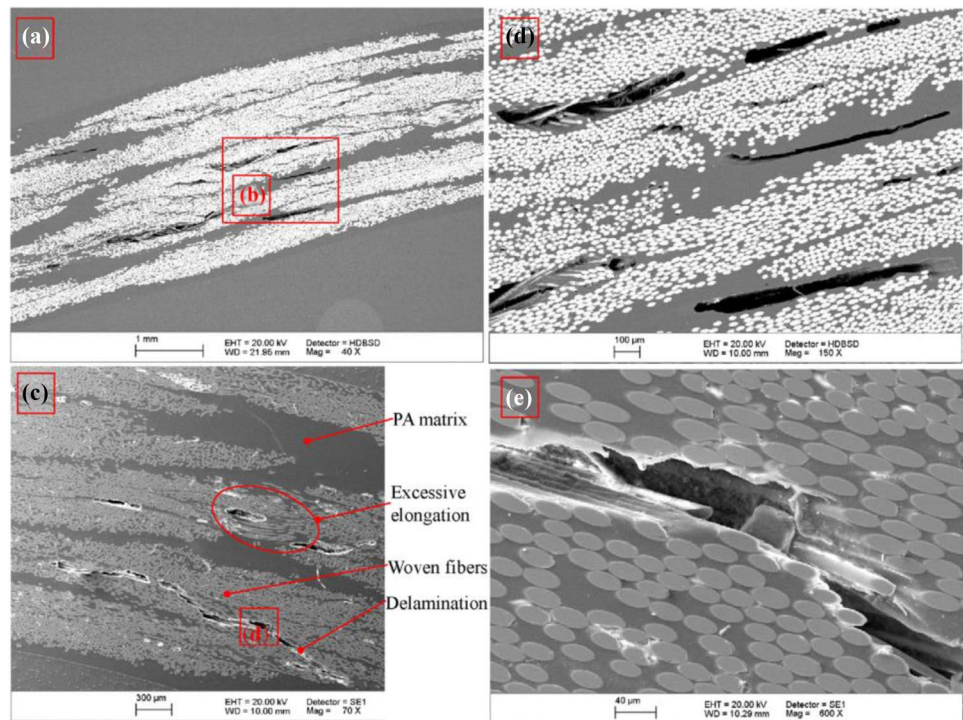
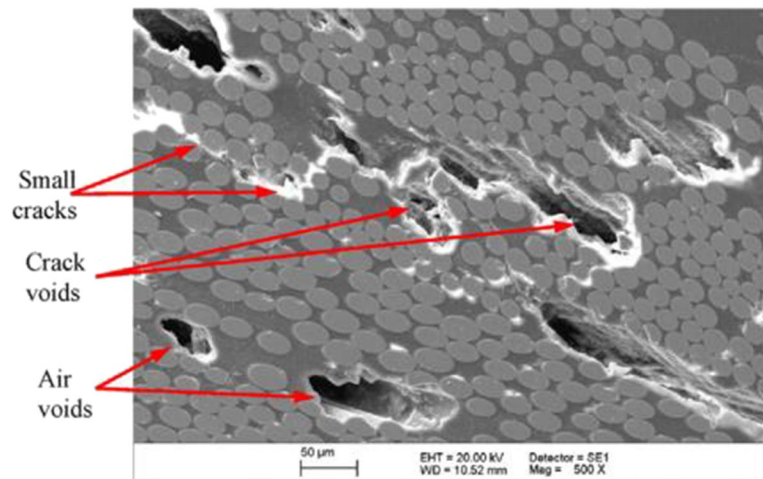


**Fig. 16** Cracks and voids in magnified SEM image [76]



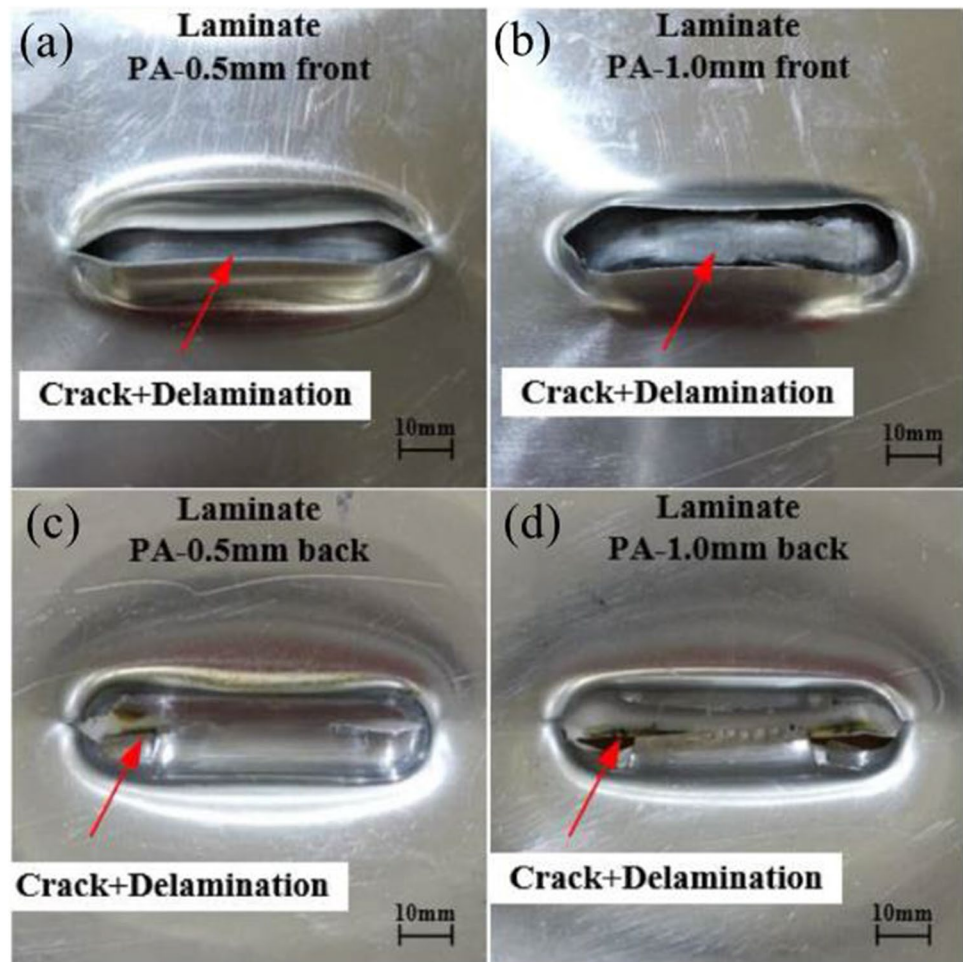
anti-failure ability. Figure 17 a and b have shown that only the cracking of Al layer with serious delamination occurred when the PA layer contacted the tool under the 2D groove deformation path, and a similar phenomenon could be observed in Fig. 18 c and d when the Al layer contacted the tool under 3D truncated-cone deformation path. The failure mode of cracking in two layers with serious delamination could be found when the Al layer faced the tool under the 2D groove deformation path.

Davarpanah and Malhotra [85] investigated the influence of the thickness of the Al layer and PA66 layer on the failure modes of PA66-Al composite sheets when the PA66

layer was in contact with the tool. Figure 19 shows the three failure modes including delamination at the metal-polymer interface, the Al-layer tearing along the circumferential direction, and the PA66 layer galling in contact with the forming tool. The results indicated that the failure mode with a small thickness of the PA66 layer and Al layer was delamination, while the failure mode with a large thickness of the PA66 layer and a small thickness of Al layer was metal tearing. This phenomenon might be due to lesser bending in the unformed region (central region) of the thicker PA66 layer, which reduced the risk of PA66 layer and Al layer interface separation, thereby reducing the possibility of delamination.



**Fig. 17** Failure modes of PA-Al composite sheets under 2D groove deformation path with  $d=20$  mm [84]



The failure mode of galling occurred in the condition of the thick Al layer and PA66 layer.

#### 4.6 Failure analysis of other composite materials

AL-Obaidi et al. [87] developed a hybrid laminate that combined an aluminum sheet with basalt fiber-reinforced thermoplastic polyamide 6. The failure modes of the hybrid laminate are delamination and void. It could be seen in Fig. 20 of zone I that the percentage of voids and delamination rate was increased with a larger profile wall angle. The greatest delamination was observed between the aluminum plate and BFRP because the plastic properties of the aluminum sheets were different from those of the BFRP during the forming process. A higher percentage of voids and delamination was observed in zone I because the laminates underwent much greater stress in zone I than in the other two zones.

Hernández-Avila et al. [32] found the appearance of wrinkles on the cone walls of the parts, as shown in Fig. 21. In their study, compared with the spindle speed of 0 rpm, more wrinkles were observed in the samples manufactured with the spindle speed of 2000 rpm, which was due to the

increase of the sheet temperature caused by the spindle speed. Furthermore, Franzen et al. [106] found that wrinkles were more common in conical parts, where it was difficult to withstand the twisting of radial cross-section caused by the motion of the forming tool. The wrinkle was related to the twist of the radial cross-section plane which was triggered by the movement of the forming tool along the helical tool path, which was expected to start in thinner sheet parts [97]. As stated by Yang et al. [107], the increase of wall angle led to the obvious increase of the appearance wrinkle.

## 5 Numerical modeling and simulation

Due to the high localization and non-linearity, it is difficult to understand the deformation mechanics of the ISF process only through experiments. Therefore, numerical simulation of the ISF process is essential to understand the deformation behaviors, process investigation, and its optimization [22]. Since there are few studies on the numerical simulation of fiber composites and



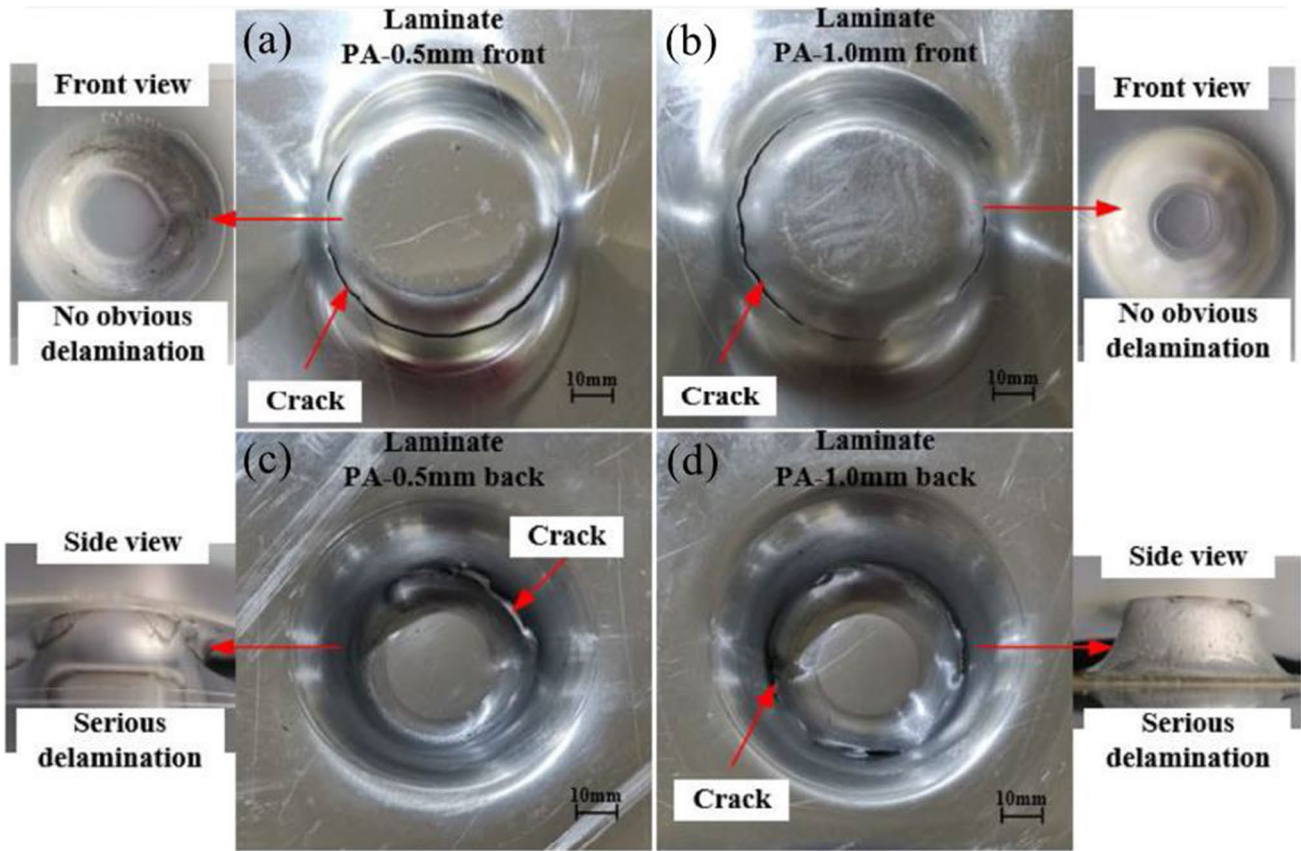
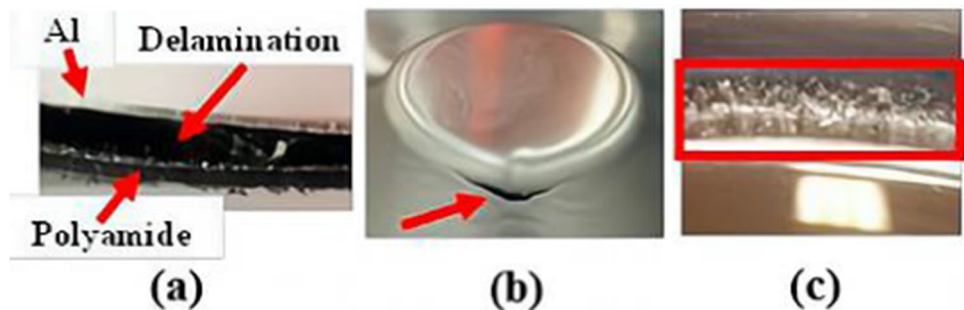


Fig. 18 Failure modes of PA-Al composite sheets under 3D truncated-cone deformation path with  $d = 20$  mm [84]

Fig. 19 Modes of failure. (a) Delamination, (b) metal tearing, and (c) galling [85]



other composites, this section mainly involves the constitutive models and finite element simulation of metal composites.

### 5.1 Constitutive models

The constitutive law has a great influence on the correct prediction of deformation and failure behavior of materials. This section reviewed the constitutive models commonly used for single-layer sheets and composite sheets.

#### 5.1.1 Constitutive models for single-layer sheet

Different material constitutive models were tested during the single-layer sheet simulation in SPIF. Some commonly used constitutive models are introduced. Other special constitutive models including the Kim–Tuan model, modified Mohr–Coulomb (MMC3) model, CPB06 constitutive model, and Cowper–Symonds constitutive model could be referred to Ref. [108], Ref. [109], Ref. [110], and Ref. [111].

For simplicity of the finite element simulation, many researchers only used the hardening law as the material

**Fig. 20** The half-formed conical shape and divided into three enlarged zones [87]

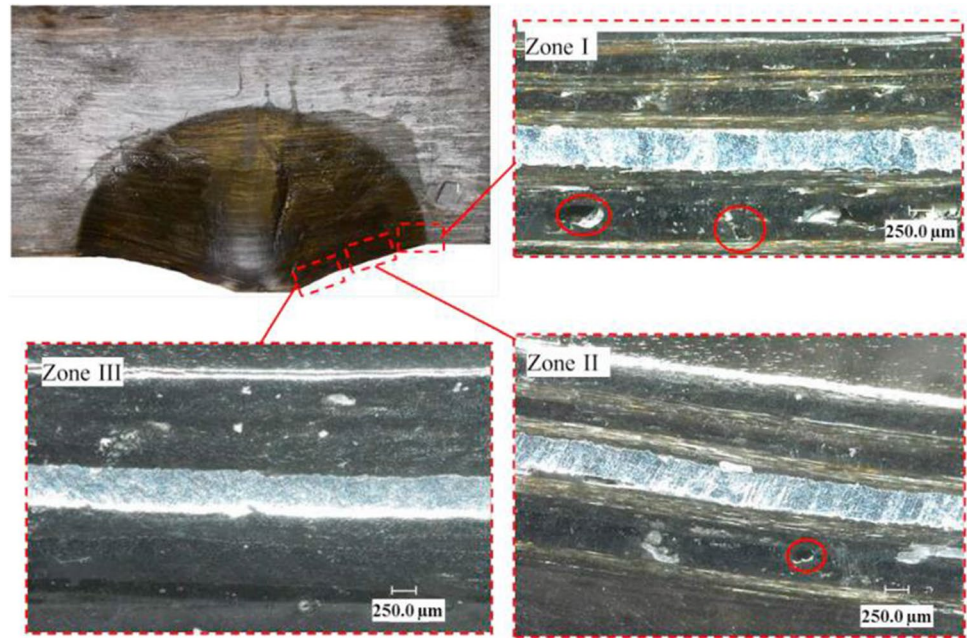
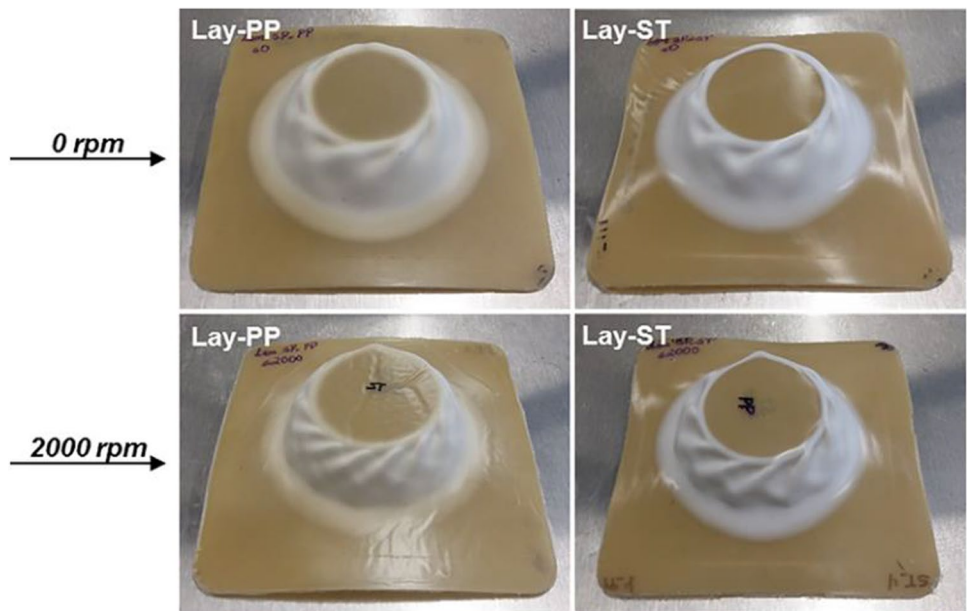


**Fig. 21** Cone-shaped parts fabricated from bilayer sheets of PP–ST [32]. (Lay-ST is referred to the bilayer sheet in which the ST is in contact with the forming tool)



constitutive law. The hardening law, also known as the flow stress law of materials, refers to the flow stress  $\sigma$  that is a function of the real strain  $\epsilon$ . This function approximates the flow stress curve measured. The widely used hardening laws include the power law (the Holloman hardening law), the Swift hardening law, the Voce hardening law, and the Ludwik hardening law.

The power law is the most commonly used hardening law in single-layer metal materials, which indicates that the material grows in the form of a power of constant hardening coefficient during the whole process of deformation. The equation can be expressed as follows:

$$\sigma = K\epsilon^n \quad (4)$$

where  $K$  is the strength coefficient and  $n$  is the work hardening exponent. The power law is widely used for the numerical simulation of single-layer metal materials, such as aluminum alloy sheets [112–125], magnesium alloy sheet [126, 127], steel sheets [128, 129], titanium alloy sheets [129], and Cu sheets [130].

The Swift hardening law can be given by the following commonly used formula:

$$\sigma = K(\epsilon_0 + \epsilon_p)^n \tag{5}$$

in which  $K$  is the strength coefficient,  $n$  is the work hardening exponent, and  $\epsilon_p$  and  $\epsilon_0$  are the equivalent strain and yield strain respectively. By summarizing the previous papers, the Swift hardening law can also be applied to the finite element simulation for the ISF processing of aluminum alloy sheets [131, 132], steel sheets [133, 134], and magnesium alloy sheets [135].

The equation of the Voce hardening law is as follows:

$$\sigma = \sigma_s + K(1 - e^{-t\epsilon_p}) \tag{6}$$

where  $K$  is the strength coefficient,  $t$  is a material parameter, and  $\epsilon_p$  is the equivalent strain. To make the hardening behavior of the aluminum alloy sheets more suitable for the ISF process, Shamsari et al. [136], Nourmohammadi et al. [137], and Ai et al. [138] implemented the Voce hardening law. In order to accurately simulate the water jet incremental microforming process, the Voce hardening law was implemented to explain the work hardening behavior of the stainless-steel foil by Shi et al. [139].

Some scholars used the Ludwik hardening law to describe the hardening behavior of materials, such as Wen et al. [140] and Movahedinia et al. [141]. The equation can be given as follows:

$$\sigma = \sigma_s + K\epsilon^n \tag{7}$$

in which  $K$  is the strength coefficient,  $n$  is the work hardening exponent, and  $\sigma_s$  is the yield stress.

To simulate the deformation behavior of materials more accurately, many scholars combine the yield criterion with the hardening law. The common combinations include the isotropic hardening law with the Von Mises yield criterion [142, 143], the isotropic hardening law with the Hill’s 1948 yield criterion [144, 145], the Holloman hardening law with the Von Mises yield criterion [146], the Voce hardening law with the Von Mises yield criterion [147, 148], the Swift hardening law with the Von Mises yield criterion [149–154], and the Swift hardening law with the Hill’s 1948 yield criterion [155, 156].

Besides, the Johnson–Cook material model is a constitutive law for predicting the plastic flow stress, which is related to the given temperature conditions, strain as well as strain rate. This model can be implemented by the following equation:

$$\sigma = (A + B\epsilon_p^n)(1 + C \ln \frac{\dot{\epsilon}}{\dot{\epsilon}_0})(1 - T^m) \tag{8}$$

where  $\epsilon_p$  is the equivalent strain, and  $A$ ,  $B$ , and  $C$  are the yield stress, the hardening modulus, and the strain rate coefficient respectively.  $\dot{\epsilon}_0$  denotes the reference strain rate,  $n$  is the hardening exponent,  $m$  is the temperature exponent, and

$T$  is the homologous temperature. The constitutive law is not only applied in ISF at the room temperature [157–159], but also used in ISF of sheet metal preheated at different temperatures [160], electric hot ISF [161–164], and laser heating ISF [165, 166].

Henrard et al. [167] compared the ability of several constitutive models to predict forming forces. The authors concluded that the material model with the highest prediction accuracy of forming force was the von Mises yield criterion with the mixed isotropic–kinematic (Voce–Ziegler) hardening model. Esmaeilpour et al. [168] applied the Voce hardening law with three different yield criteria including Barlat Yld2004-18p, Hill’s 1948 and von Mises criterion to simulate the SPIF process of the AA7075-O sheet. The results have shown that the forming quality of the conical parts simulated by the three yield criteria is very similar, but the calculation time of the Barlat Yld2004-18p criterion is the longest, while the calculation time of the von Mises criterion is the shortest. Han et al. [169] studied the influence of different yield criteria (von Mises and Hill48) and hardening laws (Armstrong–Frederick, isotropy, and kinematics) on the prediction accuracy of straight flanging by ISF. They drew a conclusion that the Hill48 yield criterion with the Armstrong–Frederick hardening laws after correction had the best prediction accuracy of sectional shape and forming force in different yield criteria, correction methods, and hardening laws.

There are relatively few papers on material damage models, which may be due to the complexity of material damage constitutive models, which also increases the time required for simulation. As reported by Said et al. [170], the constitutive model based on quadratic yield criteria of Hill’48 with the mixed isotropic/kinematic hardening law could predict ductile damage in SPIF more accurately compared with the isotropic hardening law. Jin et al. [171] proposed an elastoplastic constitutive model which combined a mixed isotropic kinematic hardening law with the Lemaitre damage model to accurately predict the deformation and formability of the sheet metal in the ISF process. Basak et al. [172] utilized the Hill’48 plasticity theory to modify seven different plastic damage models. The Bao–Wierzbicki fracture criterion incorporating the Hill48 anisotropic yield model was considered to be the most appropriate model to predict the fracture behavior of AA6061 material during the ISF process because its average error is the smallest. According to the study of Gatea et al. [173, 174], the GNT damage constitutive model was applied to predict the effects of main parameters on the formability and fracture of titanium sheets in the ISF process. Guzmán et al. [175] applied the modified GTN model which was extended to shear to predict the damage during SPIF. They came to a conclusion that the predicted maximum forming angle is smaller than the actual maximum forming angle for complex parts like the cone.



### 5.1.2 Constitutive models for composite materials

For the numerical simulation of ISF, the constitutive law of composite materials can usually be inherited from the constitutive law of single-layer materials. The constitutive law of Al–St [38, 40], Cu–Al [43, 46–48], St–Ti [51, 52], and St–St [54] composite materials is the isotropic hardening laws. Bouhamed et al. [50] first used the Mori–Tanaka model to estimate Young’s modulus, density, and Poisson’s ratio of Ti–Al composite sheets containing different volume fractions of Ti particles, and then applied RVE to obtain the Ludwik hardening law’s parameters of Ti–Al composite sheets containing different volume fractions of Ti particles. Finally, the finite element method is applied to simulate the ISF process of composite sheets based on the obtained material properties data. For the finite element simulation of the FSTWBs as shown in Fig. 22, Marathe et al. [176] applied the isotropic hardening law to simulate the SPIF process. Sakhtemanian et al. [53] used a modified Johnson–Cock material constitutive model to investigate the influence of ultrasonic vibration on the SPIF process of St–Ti composite sheets. Wu et al. [93] applied the Johnson–Cock constitutive model to numerically simulate the friction stir–assisted ISF process of synchronously bonding Al–St composite sheets.

The constitutive models mentioned above are mainly aimed at metal materials. Due to less research on ISF of fiber-reinforced composites, there are few examples of finite element simulation. However, we can refer to the constitutive models of fiber-reinforced composites in stamping [177, 178] and impacting [179]. For example, Liu et al. [177]

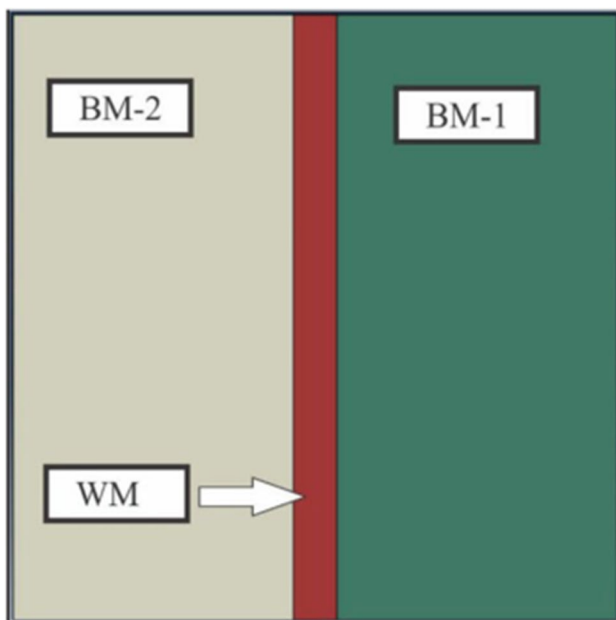


**Fig. 22** The simulation of the sheet (BM and WM represent the base metal and welding material respectively) [176]

used a non-orthogonal constitutive model to characterize the anisotropic material behavior of GFRP in thermostamping process. A convected coordinate system, whose in-plane axes are coincident with the weft and warp yarns of woven fabrics, is embedded in the shell elements. Contravariant stress components and covariant strain components in a constitutive relation are introduced into the convected coordinate system. The transformations between the contravariant/covariant components and the Cartesian components of the stress and strain tensors provide a method for deriving the global non-orthogonal constitutive relations for woven composite fabrics. By taking advantage of the tensile–shear decoupling in the constitutive equation under the convected coordinate system, the material characterization of woven fabrics is simplified. Tang et al. [179] established a mechanical model based on the CFRP laminates, which considers the effect of hygrothermal diffusion on a ballistic impacting process. The model solves the Luikov equations by means of the differential quadrature method. The failure and partial failure of a projectile with high velocity into the composites were studied based on the conservation of energy. Further, as hygrothermal deformation reaches equilibrium, the effect of hygrothermal effects on the ballistic impact event was investigated.

### 5.2 Finite element modeling

Since the finite element simulation of other composite materials has not been found, this section mainly introduces the finite element simulation of metal composite materials and fiber-reinforced materials. How to simulate the composite sheet is an important aspect of the finite element analysis of composite materials.

In the finite element modeling of composite materials, explicit analysis and shell elements are widely applied because they can greatly reduce computation time. Although both shell element and solid element have the ability in predicting the displacement field, the shell elements cannot accurately predict the stress/strain field in the thickness direction. Therefore, a detailed study of SPIF requires the use of three-dimensional solid elements [94].

For multi-layer metal composite materials, the most common approach is to define a section for each single layer. The material properties of each sheet were assigned to each section. Then, both sections were attached using the tie constraint [47, 51–53]. To simulate the delamination phenomenon on SPIF of the steel–steel composite sheet, Hassan et al. [54] used the surface-based cohesive interaction to simulate the interface between two St sheets. Qin et al. [48] adopted a similar method for Cu–Al composite sheets. Solid elements C3DR8 were used to simulate the Cu layer and Al layer, while cohesive elements COH3D8 were adopted to simulate the interface, as shown in Fig. 23. And the determination



**Fig. 23** Finite element model of the Cu-Al composite sheet [48]

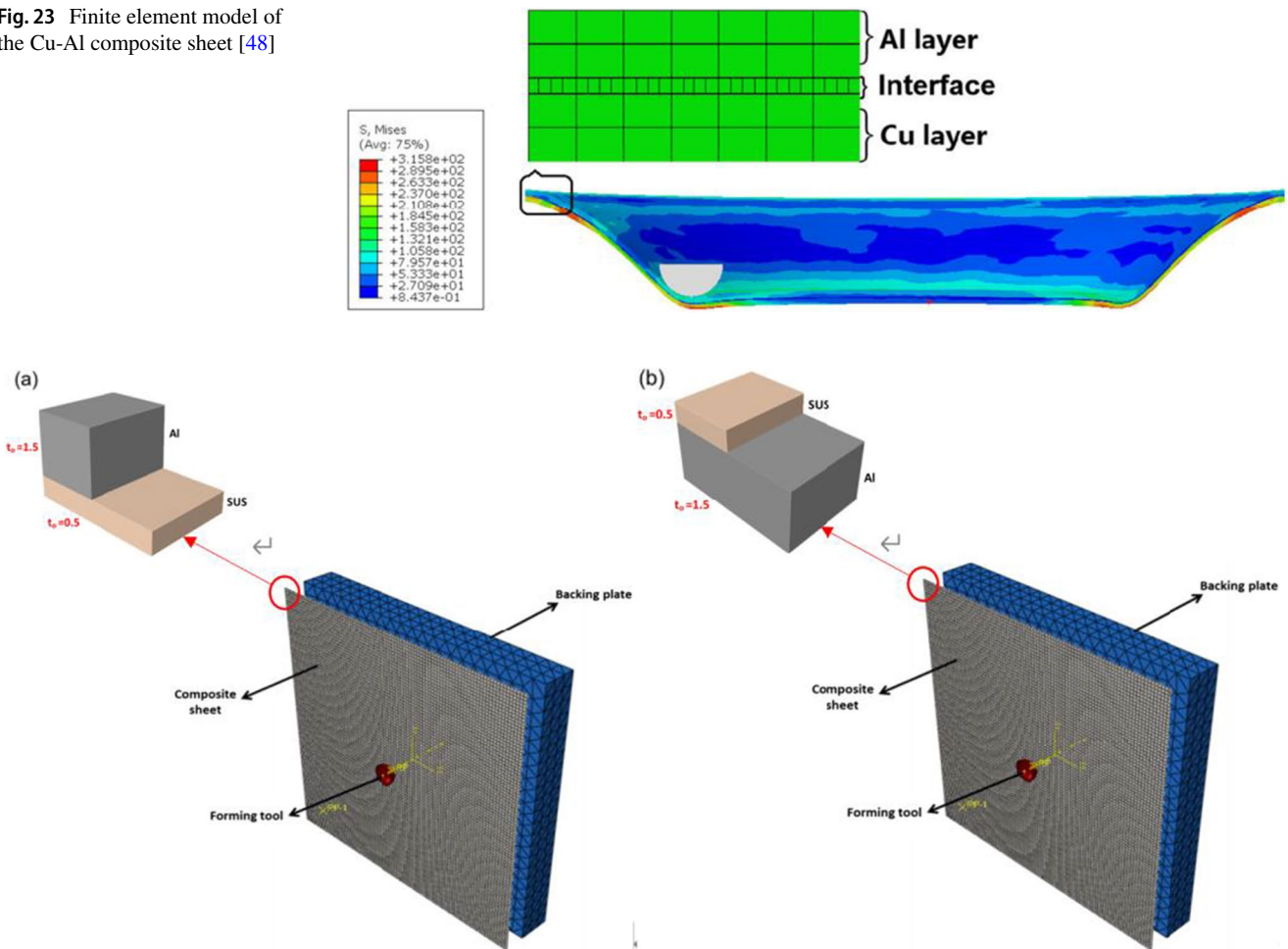


**Fig. 24** The layer arrangements of Al-St composite sheets. (a) Al/St and (b) St/Al [38]

of the cohesion element parameters was also explained in detail.

Abd Ali et al. [38] selected a composite layup choice to simulate the Al-St composite sheet. The two types of layer arrangement are shown in Fig. 24. To simulate the FSTWBs, Marathe et al. [176] divided the sheet into three sections in the horizontal direction, as shown in Fig. 22. Then, the material properties of each section were assigned. The properties of the welding material were the average of the two base metals. Liu et al. [43] applied a new method that defined the composite sheet as a whole. The mechanical properties of the Cu-Al composite sheet including Young’s modulus, Poisson’s ratio, yield stress, and ultimate tensile strength can be calculated by the equation in Ref. [180], as shown below

$$\alpha_{Cu-Al} = w_{Cu}\alpha_{Cu} + w_{Al}\alpha_{Al} \tag{9}$$

where  $\alpha_{Cu-Al}$ ,  $\alpha_{Cu}$ , and  $\alpha_{Al}$  refer to the Young’s modules, Poisson’s ratios, yield stresses, and ultimate tensile strengths.  $w_{Cu}$

and  $w_{Al}$  are the percentage fractions of metallic components in a composite sheet.

Xiao et al. [80] built a FE model of the CFRP sheet in the ISF based on the mesoscopic scale. Each bundle of carbon fiber was simulated by the yarn which was drawn by CATIA software and imported into ABAQUS for assembly, and each bundle of yarn is assigned material properties. Figure 25 shows the mesoscale model used to simulate the fabric and discrete rigid tool surfaces, using a quarter geometry to reduce simulation time.

Due to the scarcity of finite element simulation for fiber-reinforced composite materials in ISF, this section also introduces the simulation of fiber-reinforced composite materials in other forming process for reference.

In order to simulate the stamping process of carbon fiber-reinforced polypropylene sheets, Wang et al. [181] established a finite element model as shown in Fig. 26. In the finite element model, shell elements S4R were used to simulate CFRP sheets, and the full CFRP sheet was divided into 5700 elements. The punch and holder were defined as

**Fig. 25** The mesoscale model used to simulate the ISF of the CFRP sheet [80]

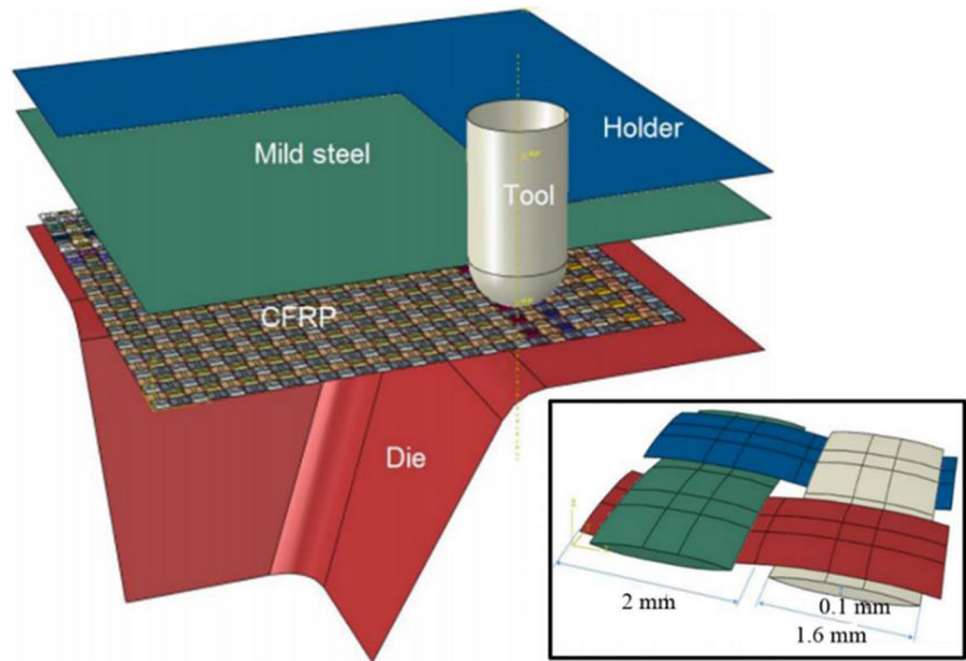
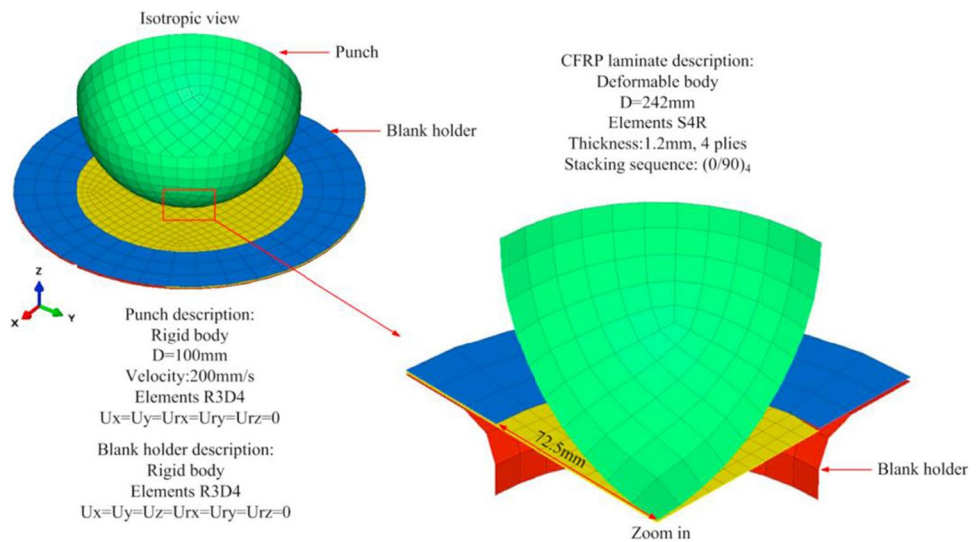


**Fig. 26** The finite element model for stamping process of CFRP sheets [181]



rigid bodies and meshed using R3D4 elements with dimensions of  $15 \times 15$  mm.

To reproduce the impact experiment of the CFRP laminate, Kazemi et al. [182] established the finite element model as shown in Fig. 27. The mesh size of the impact zone of the CFRP laminate is  $0.25 \times 0.25$  mm, and the coarse mesh is used in other areas. In order to simulate the initiation and development of delamination in the interface between adjacent plies of the laminate, the model applied a surface-based cohesive contact method. Figure 28 illustrates the schematic of the load transfer behavior of the surface-based cohesive contact method.

Fu et al. [184] established a finite element meso model of CFRP sheets to analyze the mechanism of induction heating of plain weave as shown in Fig. 29. Based on the finite element mesoscopic model, the induction electricity-magnetic-eddy current-temperature multi-field coupling analysis model of plain weave CFRP is established. The coupling and distribution rules of the electro-magnetic-eddy current field during induction heating were studied. Furthermore, the heating history and temperature distribution of carbon fiber composite materials during heating were analyzed, and the correctness of the finite element mesoscopic model was verified through experiments.

**Fig. 27** The finite element model for impacting test of the CFRP laminate [182]

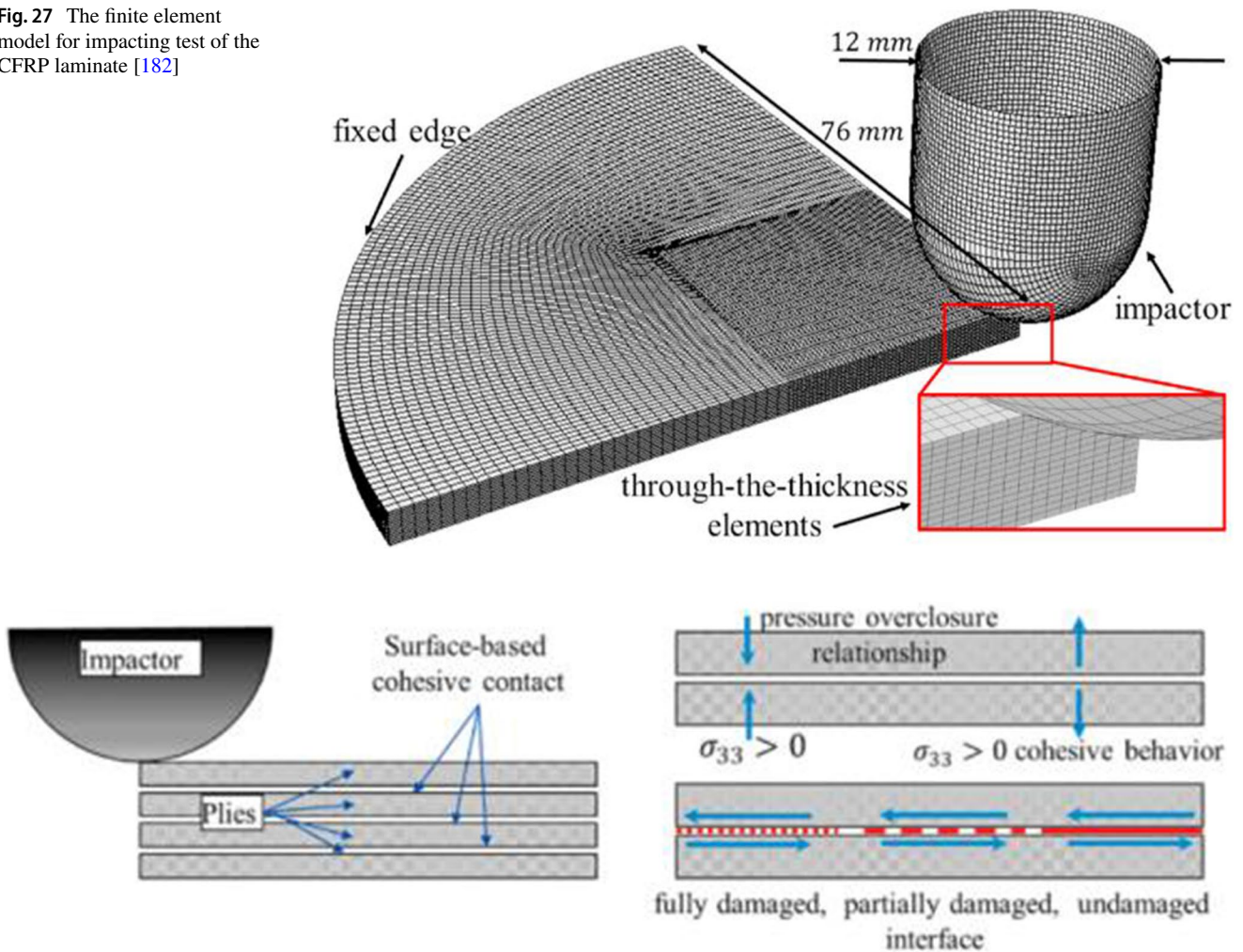


**Fig. 28** The schematic of load transfer behavior of surface-based cohesive contact method [183]

## 6 Formability of composite materials

### 6.1 Formability evaluation

The formability of composite materials in ISF is often characterized by the maximum drawing angle and the maximum forming depth. When the selected geometry of the part is a frustum pyramidal shape that has variable wall angles along the forming depth [38, 39, 77] or a truncated cone with variable generatrices [43, 60, 61], the maximum drawing angle is regarded as an indication of formability. When two shapes (groove [43, 44] and truncated cone with variable generatrices [47, 89]) are selected, the maximum forming depth is regarded as an indicator to characterize the process formability of composite materials. The influence of parameters on the maximum drawing angle and the maximum forming depth was studied by changing the process parameters.

FLDs are also used to characterize the formability of composite materials in the ISF process. The limit strain of the fault area is an important part of an FLD. According to the study of Abd Ali et al. [38], the FLD was applied in ISF to investigate the formability by using major and minor strains of Al-St composite sheets. Figures 30 and 31 describe the influence of step size, layer arrangement, and tool diameter on the FLD. To measure the major and minor strains on the external layer of the composite sheets after ISF, two sections were created on the external layer, including two deformation modes, namely biaxial stretching in the corners of formed parts and plane strain at the wall of the formed part. The fracture strains were obtained according to the method used in the research of Centeno et al. [185]. The FFL was acquired based on the SPIF process of the truncated pyramid shape, which was one of the shapes suggested by Isik et al. [186]. For both layer arrangements, the maximum strain on the external layers was measured with the condition of small tool diameter



**Fig. 29** Process chart for establishing a meso geometric model [184]

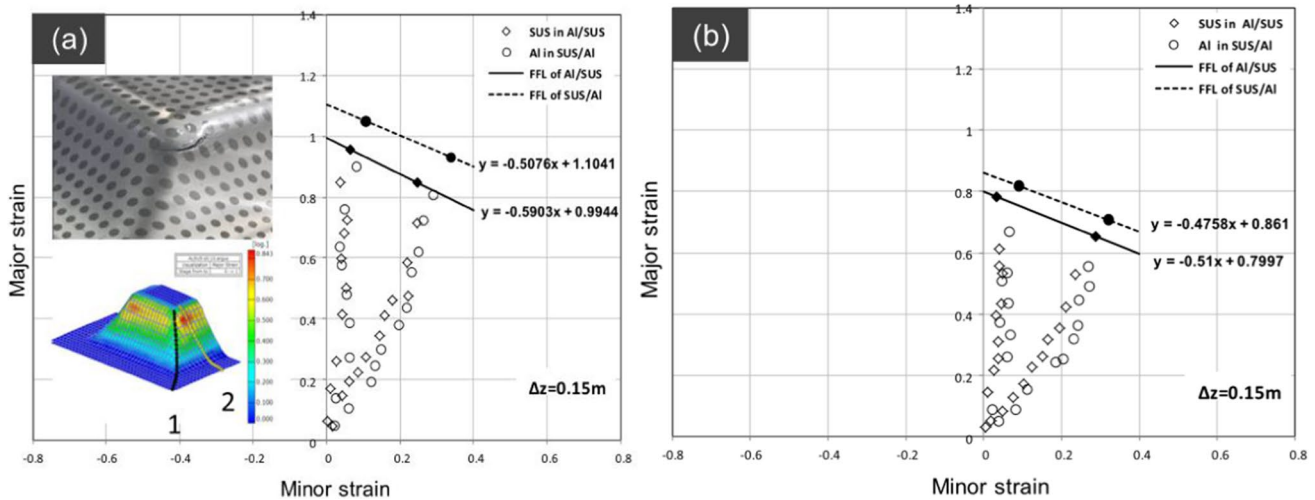
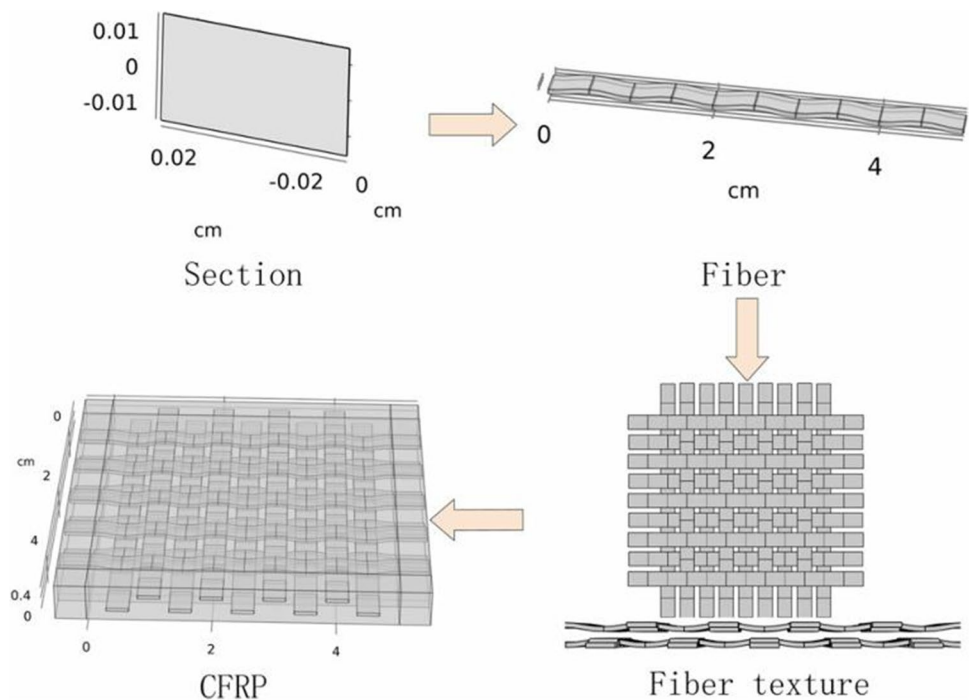


**Fig. 30** FLD for both layer arrangements with  $\Delta z = 0.15$  mm. (a)  $d = 10$  mm and (b)  $d = 20$  mm [38]

and small step size, which is shown in Fig. 30a. Moreover, the major strain of the St/Al layer arrangement was larger than that of the Al/St layer arrangement under the same conditions. In the case of the same layer arrangement, increasing the tool diameter and step size led to a slight improvement in formability. Therefore, according to the maximum stable strain before fracture, the method to promote the formability of the Al-St composite sheet was determined. In both conditions of parameters in Fig. 30 and Fig. 31, the necking before fracture of both layers

was observed. The layer arrangement is a very important parameter affecting the formability of metal composite sheets. Therefore, under different parameters, the fracture with necking of composite sheets for both layer arrangements is more obvious than that of the monolithic sheets, and Silva et al. [187] observed the same trend in the case of the large tool diameter. But, Centeno et al. [185] found that the behavior under the two tool diameter ranges was same, which meant that the failure mechanism of metal composite sheets is the same as that of the single-layer metal sheets.

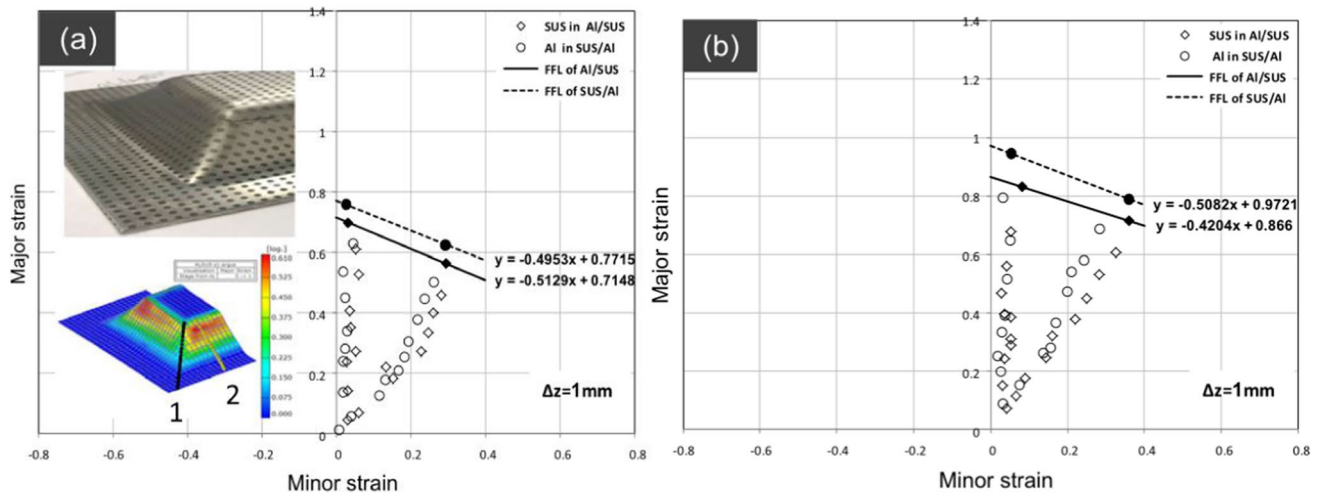


Fig. 31 FLD for both layer arrangements with  $\Delta z = 1$  mm. (a)  $d = 10$  mm and (b)  $d = 20$  mm [38]

## 6.2 Effects of process parameters

It was reported that the tool radius, spindle speed, feed speed, initial sheet thickness, step size, forming temperature, and wall angle are important process parameters, which affect the formability of composite materials in ISF. Except for fiber-reinforced composite materials, the layer arrangement is also a very important process parameter that affects the formability.

### 6.2.1 Tool radius

Tool radius is considered a significant process parameter in ISF of composite materials, which has been extensively studied. As reported in Abd Ali et al. [38], they found that the increase of the tool radius reduced the formability of the Al-St composite sheet in ISF, which was the same as the case of monolithic metal sheets, and a similar conclusion was also derived by Raneen et al. [39] and Liu and Li [43]. According to the studies by Ghamdi and Hussain [58], the formability of composite sheets was reduced with the increase of the tool radius. The authors mentioned that if the tool size was further increased, it tended to approach the stamping formability because this will enlarge the deformation area and thus changing the property of deformation from local (SPIF) to global (stamping). In the study of Ashouri and Shahrajabian [56], the formability (fracture height and fracture angle) decreased when increasing the tool diameter. Larger tool diameters can result in greater tensile strain, so that the sheet metal fractured at lower heights. It can be concluded that the influence of the tool radius on the formability of the composite sheet is the same as that of the single-layer sheet.

### 6.2.2 Spindle speed

Spindle speed is also a key factor that can influence the formability of metallic composite materials during the ISF. Many researches have been carried out to study its effects. In the research of AL-Ghamdi and Hussain [61], under the conditions of small tool diameter, step size, and feed speed, as well as low annealing temperature (e.g., 6 mm, 0.2 mm, 1000 mm/min, 400 °C), the formability was improved with the increase of the rotation speed. However, when the material annealing temperature was higher (e.g., 700 °C) and the values of parameters were larger, the increase of the rotation speed decreased the formability of Cu-St-Cu composite sheets. In contrast to the monolithic sheet, the formability of composite sheets is not necessarily improved with the increase of rotation speed, since other process parameters may also affect the formability. This observation proved that the effects of process parameters were highly complex and interactive.

### 6.2.3 Feed speed

Feed speed is also an important process parameter affecting the formability of metallic composite materials. Ghamdi and Hussain [61] indicated that the formability of the composite sheet decreased with the increase of feed speed for high annealed temperature (e.g., 700 °C). In the research of Ashouri and Shahrajabian [56], with the increase of feed speed, the deformation and displacement opportunities of the material decreased, so the sheet was more prone to fracture. Liu and Li [43] came to the same conclusion in the ISF of the Cu-Al composite sheet.

### 6.2.4 Initial sheet thickness

Different from the ISF of monolithic metal sheets, the influence of the thickness of composite sheets on formability was less studied. Furthermore, for multi-layer metal composite sheets, the thickness of different layers might also be an important parameter affecting the formability, but it had not been studied. Hou et al. [77] found that the increase of initial sheet thickness led to the increase of the forming limit because the strain in the direction of thickness decreased with the increase of thickness. Okada et al. [79] came to the same conclusion when forming carbon fiber–reinforced PA6 composite sheets.

Furthermore, in the research of Davarpanah and Malhotra [85], the influence of PA66 layer thickness on the formability of PA66–Al composite sheets was studied. Their results have shown that the formability increased first and then decreased with the increase of PA66 layer thickness.

### 6.2.5 Step size

Many studies have shown that step size has a significant influence on the formability of metallic composite materials in ISF. According to the studies by Liu and Li [43], when forming the shape of a truncated cone with a variable generatrix, the increase of step size decreased the formability (maximum drawing angle), but the situation was the opposite when forming the shape of the groove. For groove tests, the larger step size resulted in more material being stored between two adjacent tool paths to withstand stronger tensile deformation, thereby enhancing the formability. However, for forming the shape of a truncated cone with variable generatrices, the larger step size led to more tensile deformation, which leads to fracture. In the research of Ashouri and Shahrajabian [56], with the step size increasing, the influence of the forming tool on the sheet from one path to another becomes larger and larger, and the material displacement is greater than that of the smaller step size, so the formability of bilayer hybrid brass–St13 sheets decreased. However, Conte et al. [74] and Torres et al. [78] came to the opposite conclusion. The better formability in the ISF of glass fiber–reinforced PA6 and linen fiber–reinforced Solanyl composite sheets was obtained when forming at a higher step size.

### 6.2.6 Forming temperature

For composites, especially fiber-reinforced composites, the temperature has a great effect on the properties of the materials. Therefore, the forming temperature is a parameter that cannot be ignored in the ISF process. In the research of Hou et al. [77], when the temperature was higher than the melting point, the decrease of

the forming temperature reduced the formability of the jute fabric–reinforced PLA composite sheets, because the thermal stability of the PLA matrix will soon be lost if the temperature is too high. Conte et al. [74, 75] concluded that the formability of glass fiber–reinforced PA6 composite sheets increased with increasing the forming temperature. In the study of Torres et al. [78], the high forming temperature decreased the formability of the linen fiber–reinforced Solanyl composite sheets.

### 6.2.7 Wall angle

The wall angle is also a very important parameter affecting the formability, but it is rarely studied in the ISF of composites. In the study of Torres et al. [78], the larger wall angle decreased the formability of linen fiber–reinforced Solanyl composite sheets. Conte et al. [74, 75] concluded that the formability of glass fiber–reinforced PA6 composite sheets decreased with increasing the wall angles.

### 6.2.8 Layer arrangement

For multilayer composites, layer arrangement is a process parameter worthy of studying. Abd Ali et al. [38, 39] indicated that the layer arrangement of Al–St influences the forming force during the SPIF process of composite sheets. When the forming tool was in contact with a harder material, the forming force is less than the opposite. Thus, better formability could be obtained when the stiff but thin layer (St layer) is contacted with the forming tool. Ashouri and Shahrajabian [56] came to a similar conclusion that the formability of the St13 layer in contact with tools was better than that of the brass layer because the formability of St13 was higher than the brass sheet. Honarpisheh et al. [47] reported that the formability with Cu/Al layer arrangement was better than that of Al/Cu layer arrangement. However, Liu and Li [43] drew a different conclusion. Compared to the Cu/Al layer arrangement, the Al/Cu layer arrangement had better formability and larger forming force because the outer thinner but stronger Cu layer was able to bear more stretching deformation. The different conclusions drawn by Liu and Li [43] and Honarpisheh et al. [47] may be attributed to the difference in the thickness ratio of the Al layer to the Cu layer. According to the study of Liu and Chen [84], the layer arrangement played a significant role in the formability of PA–Al composite sheets. Because of the weak bond between the PA layer and the Al layer and the weak PA layer, when the PA layer contacted tools, the composite sheet was easy to delaminate in the early stage of forming, which reduced the formability of the composite sheets.



## 7 Forming forces

In this section, firstly, the reason for studying the forming force is explained. And then the influence of contact conditions and process parameters on forming force of composite materials in ISF is reviewed.

Forming force is a key parameter that helps selecting suitable machine equipment and forming tools, avoiding forming damage, and reducing wear between the tool and sheet, as well as determining energy consumption and final formed shape [188–203]. It is also a significant factor in ISF that provides an understanding of the deformation mechanics, monitoring the forming process, and preventing the failure prediction.

### 7.1 Effects of process parameters

Liu and Li [43] investigated the influence of some significant process parameters, including the layer arrangements, layer thicknesses, wall angle, and tool diameter, as well as step size, on the forming force in the SPIF process of Cu-Al composite sheets. The results indicated that the forming force of Al/Cu sheets was higher than that of Cu/Al sheets and the vertical force increased as the thickness of the Cu layer in the composite sheets increased. In addition, they found that the vertical forming force increased with increasing the tool diameter and step size, while the vertical forming force first increased and then decreased with increasing the wall angle. Haghpanahi et al. [46] and Gheysarian et al. [45] agreed with the results that the increase of step size and tool diameter increased the vertical forming force. Moreover, Haghpanahi et al. [46] also found that the greater the thickness of the composite sheets, the greater the forming force. Hernández-Avila et al. [32] and Lozano-Sánchez et al. [92] came to the same conclusion that the increase of spindle speed decreased the forming force, which was attributed to the softening of the sheet due to the heat generated by friction between the forming tool and the sheet when forming PP-ST composite sheets and PP-MWCNTs composite sheets, respectively. Sakhtemanian et al. [51, 52] indicated that the increase of step size had a negative effect on the forming force of St-Ti composite sheets, which was due to the increase of the work hardening caused by the application of the higher step size. In another work [53], they found that the application of ultrasonic vibration significantly reduced the forming force because the ultrasonic vibration reduced the friction coefficient between the tool and the sheet surface, and increased the temperature of the sheet which led to the decrease in the flow stress of the materials. Ghassabi et al. [40] found that for the ISF of Al-St composite

sheets, the spindle speed does not affect the forming force, and the feed speed only has little effect on the forming force. Davarpanah and Malhotra [85] found that the large thickness of the PA layer would increase the forming force while the large thickness of the Al layer did not affect forming force for PA66-Al composite sheets.

## 8 Forming quality

The forming quality is mainly assessed through the shape (forming accuracy, surface quality) and performance (strength, fatigue) of the final formed composite material parts.

### 8.1 Forming accuracy

The forming accuracy of single-layer sheets in ISF has been investigated extensively [204–220]. There are few works on the forming accuracy of composite parts in ISF, but it is very important to ensure the forming accuracy of composite parts manufactured by the ISF process meets the requirements. Forming accuracy is the difference between the expected/ designed geometry and the formed geometry of the composite materials after ISF.

Romina et al. [74] observed that the forming accuracy of composite parts could be improved by increasing the step size and forming temperature. As investigated by Ghassabi [40], the spindle speed and economic speed did not affect the accuracy, but the large step size decreased the accuracy and the tool path also affects the forming accuracy of the part. Li et al. [42] found that the layer arrangement of aluminum alloy and steel composite sheets had a great influence on the forming accuracy of parts. Since AA5052 is more prone to material flow than DC05 at high temperatures, Al/St layer arrangement tends to have a higher bulge structure than the St/Al layer arrangement; that is, the accuracy of the St/Al layer arrangement is higher.

### 8.2 Surface quality

Surface quality in ISF is mainly characterized by the values of surface roughness [221–235]. In general, the surface roughness is obtained by measuring the morphology of the surface with a profilometer.

In general, the use of lubricants can reduce the friction between the tool and the workpiece to improve the surface finish. The grease and liquid lubricants are generally used types of lubricants for composites in the ISF. In addition to suitable lubricants, certain forming parameters also affect the surface finish. In the research of Wei et al. [57], a combination of parameters named  $d \sin \theta / 2pt$  (where  $\theta$  is the forming angle,  $d$  is the tool diameter,  $p$  is the step size, and  $t$  is

the sheet thickness), which had a controlling effect on the roughness of the inner surface, was proposed. The value of surface roughness decreased with the increase of parameter combination value. To produce high-quality Cu-St composite sheets, it is recommended to maintain an optimal value of  $20 \text{ mm}^{-1}$ . Hou et al. [77] found that reducing the step size increased the surface quality of the formed composite part when the forming depth was large. The results of Liu and Li [43] showed that the values of surface roughness of Cu-Al composite sheets in the SPIF could be obtained by the small step size, the large diameter of forming tool, and large initial drawing angle. In the research of Sakhtemanian et al. [52], the scratches on the sample surface became deeper and the quality of the sample surface decreased by increasing the step size, which was consistent with the conclusion of the aluminum alloy sheet investigated by Liu et al. [236]. Similar to the results of Raneen et al. [39], Gheysarian and Honarpisheh [45] found that the large diameter of forming tool and small step size decreased the surface quality of metal composite parts, and the diameter of forming tool had the greatest influence on the surface roughness. The increase in tool diameter indicates that the forming quality of the part was enhanced by reducing the stress because the contact area between the forming tool and the inner layer increased [237]. With the decrease of the step size, the height between the two adjacent tool paths also became smaller, which led to the decrease of surface roughness value and the better surface quality [238–240]. For multilayer metal composites, the layer arrangement also affects the surface quality of the formed parts. As investigated by Raneen et al. [39], St/Al layer arrangement had a better surface quality than Al/St layer arrangement. In the research of Gheysarian and Honarpisheh [45], the surface roughness value of the Al/Cu layer arrangement is greater than that of the Cu/Al layer arrangement. Al-Ghamdi and Hussain [63] studied the effects of normal strain, sheet strength after forming, residual stress, and forming force on the free-surface roughness of Cu-St-Cu composite sheets in ISF. The results demonstrated that the average roughness value of the free surface increased nonlinearly with the increase of normal strain for the free surface. They also found that the roughness value on the free surface increases linearly as the sheet strength after forming, residual stress, and forming force increased. Their analysis showed that the roughness of the free surface was inversely proportional to the roughness of the contact surface and that the forming angle had the greatest influence of all parameters.

### 8.3 Mechanical strength

Tensile strength and yield strength are considered to be important indexes of the ISF-ed part because they determine the service performance of the part. In recent years,

more and more scholars pay attention to the research on the strengths of single-layer metal parts [241, 242] and polymer parts [243]. The tensile test is a common method to measure the values of strengths. The sample that was cut from the side wall of the part was used for the tensile test with the aim of obtaining the stress–strain curve and calculating the values of yield strength and tensile strength. The effects of important parameters (such as forming temperature, step size, feed speed, tool diameter, spindle speed, sheet thickness, and wall angle) on yield strength and tensile strength were investigated [244–251]. In contrast, the strength of composite materials has been less studied. Al-Ghamdi and Hussain [63] concluded that the strength of the Cu-St-Cu composite parts formed by ISF increased, which was consistent with single-layer metal materials. The research of Matsumoto et al. [91] showed that the joining strength of the PMMA sheet and the nickel foam by friction stir ISF was larger than the fracture strength of the nickel foam. According to the study of Sakhtemanian et al. [52], the tensile strength of the St-Ti composite parts increased with increasing the step size, which was attributed to the transition of the grain structure from the equiaxial state to the fibrous state and resulted in the texture formation in the microstructure. The result was consistent with the case of aluminum alloy material studied by Li et al. [245]. Wei and Hussain [65] investigated the influence of parameters on tensile strength and yield strength of post-ISF Cu-St-Cu parts by analysis of variance on the measured tensile properties. The result indicated that the wall angle and annealing temperature of the material were the most important parameters affecting yield strength and tensile strength. The mechanical strength could be promoted under the condition of intermediate values of rotation, step size, low annealing temperature, high tool diameter, and low feed rate.

### 8.4 Fatigue

The fatigue properties are the most important index to determine the service life of parts. The fatigue properties of single-layer metal materials have been studied by some scholars. Xu et al. [252] found that parts formed by the ADSIF process had longer fatigue life than the original material. According to the study of Emmens and Boogaard [253], fatigue was only slightly present in the ISF process compared to the bending tests. In the research of Agrawal et al. [254], the fatigue life of the parts manufactured by the three processes including deformation machining, SPIF, and conventional bending was compared. The conclusions indicated that the parts manufactured by SPIF had significantly longer fatigue life. Nirala et al. [255] found that the FGBIT resulted in metal parts with a higher fatigue life and better ratio of strength to weight compared to conventional

**Table 3** Effects of process parameters on different aspects of composite materials in ISF from reviewed publications

Process parameter	Resulting effects				
	Forming force	Formability	Accuracy	Surface finish	Strength
Tool radius ↑	↑ [43–46]	↑ [44, 79] ↓ [38, 39, 43, 56, 58]		↑ [39, 43, 45]	
Step size ↑	↑ [40, 43, 45, 46, 51, 52]	↑ [74, 75, 78] ↓ [38, 39, 43, 56]	↑ [74, 75] ↓ [40]	↓ [39, 40, 43, 45, 52, 77]	↑ [52] ↑+↓ [65]
Spindle speed ↑	↓ [32, 92] — [40]		— [40]	↓ [32]	↑+↓ [65]
Feed speed ↑	↓ [40]	↓ [43, 56, 61]	— [40]		↑+↓ [65]
Sheet thickness ↑	↑ [46]	↑ [77, 79]			
Forming temperature ↑		↑ [74, 75] ↓ [77, 78]	↑ [74, 75]		
Wall angle ↑	↑ [42] ↑+↓ [46]	↓ [74, 75, 78]	↓ [74, 75]		↑ [65]
Layer arrangement	Al/Cu: [43–45] St/Al: [38] Ti/St: [51] ST /PP: [32]	Al/Cu: [43] Cu/Al: [44] St/Al: [38, 39, 42] St/Ti: [51] St/Brass: [56] Al/PA: [84]		Cu/Al: [44, 45] St/Al: [39] St/Ti: [51]	

spiral toolpath. Unfortunately, there are no fatigue studies on composite materials of the ISF process.

### 8.5 Summary

According to the relevant investigations presented in the literature above, the effects of different parameters on the forming quality of composite materials are summarized to provide clearer reference information for readers. Table 3 gives detailed results of the influences of parameters on different aspects for composite materials in ISF. To be more comprehensive, the influences of process parameters on formability as well as forming force are also included in Table 3. The upward arrow (↑) represents the increase of process parameters or a positive influence on the resulting effects. The downward arrow (↓) and the horizontal line (—) mean the negative influence and the negligible influence on the resulting effects, respectively. The special mark (↑ + ↓) indicates that the resulting effects first increase and then decrease with the increase of process parameters. In the row of “Layer arrangement,” Al/Cu means that the forming force/formability/accuracy/surface finish of Al/Cu layer arrangement is larger or better than that of Cu/Al layer arrangement, and the same applies to others.

### 9 Future trends

It has been seen that the ISF proved itself as a novel flexible forming technique to produce composite material components. Many developments have been done in ISF over the

last two decades. However, there is still a lot of potential in ISF that needs to be developed to adapt it to new composite materials forming. Some of the future research trends are recommended as follows:

- New heating technology associated with the ISF can open new possibilities for processing composite materials effectively and efficiently.
- The existing theories should be modified to better explain the deformation and failure mechanisms of various composite materials processed by the ISF.
- Multi-scale numerical models are needed to understand the thermo-mechanical deformation behaviors of composite materials, especially fiber-reinforced ones.
- The physical explanations about the influences of key process parameters require further investigation based on extensive experimental work.
- During the heat-assisted ISF, the surface quality of final formed parts is a big concern, especially for metal composites since most lubricants cannot endure high temperatures. Therefore, lubrication and material wear may be a focus in the future.
- Fatigue affects the service life of formed composite materials parts. There is little work on this aspect that should be emphasized in future studies.
- Online monitoring and control platform can be established to improve the forming quality during the ISF of composite materials.

Even though ISF has developed significantly for the last two decades, various aspects like the deformation and



failure mechanisms adapted to different materials still need more understanding. A lot of studies on the ISF of composite materials have been done by various researchers at the laboratory level, but due to the low speed of processing, ISF is not popular in industrial applications. There are many applications in industries where ISF can be used instead of traditional methods without expensive dies. Hence, efforts are required to make ISF a cheaper and more industrial-friendly process in the processing of composite materials.

## 10 Conclusions

With the diversified applications of composite material parts, ISF provides a promising solution to forming such materials. However, its development is still at an early stage. In this article, we have provided an overview of the recent advancements and discussions on the scientific and technological issues in the shapes and performances of various composite materials manufactured by ISF. This forms a guideline and reference for further exploring the deformation potential of new composite materials. To have a deep understanding of ISF processing composite materials, conclusions are drawn as follows:

- Much special auxiliary equipment is applied to process composite materials that are not easy to deform at room temperature. However, in the heat-assisted ISF process, how to achieve economical and uniform heating of composite materials is still a challenge in future research. To solve this, new analytical models could be developed to predict the influence of forming temperature or ultrasonic heating on the stress distribution of composite materials in the heat-assisted ISF or ultrasonic-assisted ISF, thereby enhancing the heating and forming efficiency and quality.
- There have been a large number of papers on the deformation and failure mechanisms of the single-layer sheet (metals or polymers), but those of composite materials are more complicated. Most researches are focused on the failure mode of fracture-related deformation mechanics on a macro scale. In the future, it is necessary to develop new analytical frameworks incorporating other failure modes into deformation mechanics and taking multi-scale factors into account.
- At present, the constitutive and damage models of metal (or polymer) composite materials are similar to those of single-layer metal (or polymer) materials, whereas there are few constitutive and damage models to accurately describe and predict the material behaviors of fiber-reinforced composite materials and other composite materials in the ISF process, which leads to little attention paid to numerical studies of these composite materials. Therefore, the future focus is to develop suitable constitutive and damage models to accurately simulate and predict the thermo-mechanical deformation behavior and forming quality of composite materials.
- For single-layer sheets (metals or polymers), membrane analysis has been successfully applied in the explanation of deformation mechanics. And this method could be extended to metal or polymer composite materials. Besides, other mechanisms, such as through-thickness shear and bending under tension mechanisms, could be also considered. However, for fiber-reinforced composite materials, it is not applicable due to the obvious anisotropy. Therefore, other analytical mechanics models should be developed to characterize the deformation mechanics related to the ISF process.
- The influences of key process parameters (including step size, tool radius, feed speed, sheet thickness, and spindle speed) on formability, forming force, accuracy, and surface quality have reached an agreement by experimental methods, but the physical explanations behind these results require further investigation.
- The influences of tool diameter, spindle speed, layer arrangement and feed speed on formability, forming force, and forming quality are not always consistent, which may be due to the coupling interaction of parameters. These special cases need to be further investigated.
- The forming accuracy, surface quality, and strength of composites have been studied by some researchers, but the fatigue properties of composite materials are very scarcely investigated, which affects the service life of formed parts. The fatigue properties after the ISF would be a research focus in the future.
- In the ISF process, there are few reports on the mechanical behaviors and microstructure changes of composites, especially fiber-reinforced composites. In the future, more researches can be focused on these aspects.

**Author contribution** Zhaobing Liu: methodology, writing—review and editing, supervision, project administration. Kai Cheng: resources, writing—original draft, review, and editing. Kerui Peng: resources, writing—original draft.

**Funding** The authors would like to thank the Start-up Funds from Wuhan University of Technology and the Fundamental Research Funds for the Central Universities (WUT: 2021-JD-B1-17) for undertaking this work.

**Data Availability** All data and materials are included in this article.

**Code availability** No code is involved in this article.

## Declarations

**Conflict of interest** The authors declare no competing interests.

**Ethics approval** This article has not been published or submitted elsewhere.

**Consent to participate** The authors consent to participate in this work.

**Consent for publication** The authors consent to publish this work.

## References

- Liu Z, Li Y, Meehan PA (2013) Vertical wall formation and material flow control for incremental sheet forming by revisiting multistage deformation path strategies. *Mater Manuf Process* 28:562–571. <https://doi.org/10.1080/10426914.2013.763964>
- Verbert J, Behera AK, Lauwers B, Dufloy JR (2011) Multivariate adaptive regression splines as a tool to improve the accuracy of parts produced by FSPIF. *Key Eng Mater* 473:841–846. <https://doi.org/10.4028/www.scientific.net/KEM.473.841>
- Liu Z, Daniel WJT, Li Y, Liu S, Meehan PA (2014) Multi-pass deformation design for incremental sheet forming: analytical modeling, finite element analysis and experimental validation. *J Mater Process Technol* 214:620–634. <https://doi.org/10.1016/j.jmatprotec.2013.11.010>
- Liu Z, Li Y, Meehan PA (2014) Tool path strategies and deformation analysis in multi-pass incremental sheet forming process. *Int J Adv Manuf Technol* 75:395–409. <https://doi.org/10.1007/s00170-014-6143-6>
- Lu H, Kearney M, Wang C, Liu S, Meehan PA (2017) Part accuracy improvement in two point incremental forming with a partial die using a model predictive control algorithm. *Precis Eng* 49:179–188. <https://doi.org/10.1016/j.precisioneng.2017.02.006>
- Ebrahimzadeh P, Baseri H, Mirnia MJ (2018) Formability of aluminum 5083 friction stir welded blank in two-point incremental forming process. *P I Mech Eng E-J Pro* 232:267–280. <https://doi.org/10.1177/0954408917692370>
- Mostafanezhad H, Menghari HG, Esmaeili S, Shirkharkolae EM (2018) Optimization of two-point incremental forming process of AA1050 through response surface methodology. *Measurement* 127:21–28. <https://doi.org/10.1016/j.measurement.2018.04.042>
- Ou L, An Z, Gao Z, Zhou S, Men Z (2020) Effects of process parameters on the thickness uniformity in two-point incremental forming (TPIF) with a positive die for an irregular stepped part. *Mater* 13. <https://doi.org/10.3390/ma13112634>
- Li X, Han K, Xu P, Wang H, Li D, Li Y, Li Q (2020) Experimental and theoretical analysis of the thickness distribution in multistage two point incremental sheet forming. *Int J Adv Manuf Technol* 107:191–203. <https://doi.org/10.1007/s00170-020-05037-y>
- Zhu H, Ou H, Popov A (2020) Incremental sheet forming of thermoplastics: a review. *Int J Adv Manuf Technol* 111:565–587. <https://doi.org/10.1007/s00170-020-06056-5>
- Zhu H, Xiao D, Kang J (2019) Research on point-pressing based double-sided CNC incremental forming. *J Mech Sci Technol* 33:4389–4400. <https://doi.org/10.1007/s12206-019-0835-7>
- Zhu H, Xiao D, Kang J (2019) Research on the double-sided incremental forming toolpath planning and generation based on STL model. *Int J Adv Manuf Technol* 102:839–856. <https://doi.org/10.1007/s00170-018-03221-9>
- Moser N, Zhang Z, Ren H, Zhang H, Shi Y, Ndip-Agbor EE, Lu B, Chen J, Ehmann KF, Cao J (2016) Effective forming strategy for double-sided incremental forming considering in-plane curvature and tool direction. *CIRP Ann* 65:265–268. <https://doi.org/10.1016/j.cirp.2016.04.131>
- Zhang H, Zhang Z, Ren H, Cao J, Chen J (2018) Deformation mechanics and failure mode in stretch and shrink flanging by double-sided incremental forming. *Int J Mech Sci* 144:216–222. <https://doi.org/10.1016/j.ijmecsci.2018.06.002>
- Valoppi B, Sánchez Egea AJ, Zhang Z, González Rojas HA, Ghiotti A, Bruschi S, Cao J (2016) A hybrid mixed double-sided incremental forming method for forming Ti6Al4V alloy. *CIRP Ann* 65:309–312. <https://doi.org/10.1016/j.cirp.2016.04.135>
- Ndip-Agbor E, Ehmann K, Cao J (2018) Automated flexible forming strategy for geometries with multiple features in double sided incremental forming. *J Manuf Sci E- T ASME* 140
- Leszak E (1967) Apparatus and process for incremental dieless forming. USA Patent 3342051A
- Hagan E, Jeswiet J (2003) A review of conventional and modern single-point sheet metal forming methods. *P I Mech Eng B-J Eng* 217:213–225. <https://doi.org/10.1243/095440503321148858>
- Jeswiet J, Micari F, Hirt G, Bramley A, Dufloy J, Allwood J (2005) Asymmetric single point incremental forming of sheet metal. *CIRP Ann* 54:88–114. [https://doi.org/10.1016/S0007-8506\(07\)60021-3](https://doi.org/10.1016/S0007-8506(07)60021-3)
- Emmens WC, Sebastiani G, van den Boogaard AH (2010) The technology of incremental sheet forming—a brief review of the history. *J Mater Process Technol* 210:981–997. <https://doi.org/10.1016/j.jmatprotec.2010.02.014>
- Behera AK, de Sousa RA, Ingarao G, Oleksik V (2017) Single point incremental forming: an assessment of the progress and technology trends from 2005 to 2015. *J Manuf Processes* 27:37–62. <https://doi.org/10.1016/j.jmapro.2017.03.014>
- Li Y, Chen X, Liu Z, Sun J, Li F, Li J, Zhao G (2017) A review on the recent development of incremental sheet-forming process. *Int J Adv Manuf Technol* 92:2439–2462. <https://doi.org/10.1007/s00170-017-0251-z>
- Gatea S, Ou H, McCartney G (2016) Review on the influence of process parameters in incremental sheet forming. *Int J Adv Manuf Technol* 87:479–499. <https://doi.org/10.1007/s00170-016-8426-6>
- Lu H, Liu H, Wang C (2019) Review on strategies for geometric accuracy improvement in incremental sheet forming. *Int J Adv Manuf Technol* 102:3381–3417. <https://doi.org/10.1007/s00170-019-03348-3>
- Ai S, Long H (2019) Review on material fracture mechanism in incremental sheet forming. *Int J Adv Manuf Technol* 104:33–61. <https://doi.org/10.1007/s00170-019-03682-6>
- Liu Z (2018) Heat-assisted incremental sheet forming: a state-of-the-art review. *Int J Adv Manuf Technol* 98:2987–3003. <https://doi.org/10.1007/s00170-018-2470-3>
- Peng W, Ou H, Becker A (2019) Double-sided incremental forming: a review. *J Manuf Sci E- T ASME* 5
- Brent Strong A, Hauwiler PB (1989) Incremental forming of large thermoplastic composites. *J Thermoplast Compos* 2:122–132. <https://doi.org/10.1177/089270578900200204>
- Hauwiler PB, Strong B (1991) Incremental forming of thermoplastic composites. USA Patent 5026514
- Neugebauer R, Meinel S, Glaß R, Popp M (2010) Characterization of contact tensions during incremental forming of metal composites. *Int J Mater Form* 3:667–670. <https://doi.org/10.1007/s12289-010-0858-1>
- Fiorotto M, Sorgente M, Lucchetta G (2010) Preliminary studies on single point incremental forming for composite materials. *Int J Mater Form* 3:951–954. <https://doi.org/10.1007/s12289-010-0926-6>
- Hernández ávila M, Lozano Sánchez LM, Perales Martínez IA, Elías Zúñiga A, Bagudanch I, GarcíaRomeu ML, Elizalde LE,

- Barrera EV (2018) Single point incremental forming of bilayer sheets made of two different thermoplastics. *J Appl Polym Sci* 136:47093. <https://doi.org/10.1002/app.47093>
33. Galdos L, Sáenz De Argandoña E, Otegi N, Ortubay R (2012) Incremental forming of sandwich materials. *Key Eng Mater* 504–506:931–936. <https://doi.org/10.4028/www.scientific.net/KEM.504-506.931>
  34. Bykov AA (2011) Bimetal production and applications. *Steel Transl* 41:778–786. <https://doi.org/10.3103/S096709121109004X>
  35. Parsa MH, Yamaguchi K, Takakura N (2001) Redrawing analysis of aluminum–stainless-steel laminated sheet using fem simulations and experiments. *Int J Mech Sci* 43:2331–2347. [https://doi.org/10.1016/S0020-7403\(01\)00038-8](https://doi.org/10.1016/S0020-7403(01)00038-8)
  36. Sedighi M, Honarpisheh M (2012) Investigation of cold rolling influence on near surface residual stress distribution in explosive welded multilayer. *Strength Mater* 44:693–698. <https://doi.org/10.1007/s11223-012-9424-z>
  37. Taleb Araghi B, Göttmann A, Bambach M, Hirt G, Bergweiler G, Diettrich J, Steiners M, Saeed-Akbari A (2011) Review on the development of a hybrid incremental sheet forming system for small batch sizes and individualized production. *Prod Eng* 5:393–404. <https://doi.org/10.1007/s11740-011-0325-y>
  38. Abd Ali R, Chen W, Jin K, Bao Y, Hussein AW (2019) Formability and failure analyses of Al/SUS bilayer sheet in single point incremental forming. *Int J Adv Manuf Technol* 105:2785–2798. <https://doi.org/10.1007/s00170-019-04470-y>
  39. Abd Ali R, Chen W, Al-Furjan MSH, Jin X, Wang Z (2019) Experimental investigation and optimal prediction of maximum forming angle and surface roughness of an Al/SUS bimetal sheet in an incremental forming process using machine learning. *Mater* 12:4150. <https://doi.org/10.3390/ma12244150>
  40. Ghassabi M, Salimi M, Haghpanahi M (2018) Simulation of incremental forming processes of a pyramidal ring made of two materials. *Mech Ind* 19:313. <https://doi.org/10.1051/meca/2018025>
  41. Wu R, Li M, Hu Q, Cai S, Wang Z, Chen J (2019) Evaluation and simulation on deformation instability mechanism in laminated sheet incremental forming. *Procedia Manufacturing* 29:36–44. <https://doi.org/10.1016/j.promfg.2019.02.103>
  42. Li M, Wu R, Cai S, Chang Z, Wang Z, Chen J (2020) Experimental investigation on friction-stir-assisted incremental forming with synchronous bonding of aluminum alloy and steel sheets. *J Mater Eng Perform* 29:750–759. <https://doi.org/10.1007/s11665-020-04600-8>
  43. Liu Z, Li G (2019) Single point incremental forming of Cu–Al composite sheets: a comprehensive study on deformation behaviors. *Arch Civ Mech Eng* 19:484–502. <https://doi.org/10.1016/j.acme.2018.11.011>
  44. Honarpisheh AGM (2017) An experimental study on the process parameters of incremental forming of Al–Cu bimetal. *J Comput Appl Res* 1:73–83
  45. Gheysarian A, Honarpisheh M (2019) Process parameters optimization of the explosive-welded Al/Cu bimetal in the incremental sheet metal forming process. *IJS-T Mech Eng* 43:945–956. <https://doi.org/10.1007/s40997-018-0205-6>
  46. Honarpisheh M, Keimasi M, Alinaghian I (2018) Numerical and experimental study on incremental forming process of Al/Cu bimetals: influence of process parameters on the forming force, dimensional accuracy and thickness variations. *J Mech Mater Struct* 1:35–51
  47. Honarpisheh M, Mohammadi Jobedar M, Alinaghian I (2018) Multi-response optimization on single-point incremental forming of hyperbolic shape Al–1050/Cu bimetal using response surface methodology. *Int J Adv Manuf Technol* 96:3069–3080. <https://doi.org/10.1007/s00170-018-1812-5>
  48. Qin Q, He L, Li C (2021) Control and optimization of bulge defect in incremental forming of Cu–Al bimetal. *Int J Mater Form*
  49. Alinaghian M, Alinaghian I, Honarpisheh M (2019) Residual stress measurement of single point incremental formed Al/Cu bimetal using incremental hole-drilling method. *Int J Light-weight Mater Manuf*
  50. Bouhamed A, Jrad H, Mars J, Wali M, Gamaoun F, Dammak F (2019) Homogenization of elasto-plastic functionally graded material based on representative volume element: application to incremental forming process. *Int J Mech Sci* 160:412–420. <https://doi.org/10.1016/j.ijmecsci.2019.07.005>
  51. Sakhtemanian MR, Honarpisheh M, Amini S (2018) Numerical and experimental study on the layer arrangement in the incremental forming process of explosive-welded low-carbon steel/CP-titanium bimetal sheet. *Int J Adv Manuf Technol* 95:3781–3796. <https://doi.org/10.1007/s00170-017-1462-z>
  52. Sakhtemanian MR, Amini S, Honarpisheh M (2018) Simulation and investigation of mechanical and geometrical properties of St/CP-titanium bimetal sheet during the single point incremental forming process. *Iran J Mater Form* 1:1–18. <https://doi.org/10.22099/IJMF.2017.26024.1085>
  53. Sakhtemanian MR, Honarpisheh M, Amini S (2019) A novel material modeling technique in the single-point incremental forming assisted by the ultrasonic vibration of low carbon steel/commercially pure titanium bimetal sheet. *Int J Adv Manuf Technol* 102:473–486. <https://doi.org/10.1007/s00170-018-3148-6>
  54. Hassan M, Hussain G, Ilyas M, Ali A (2020) Delamination analysis in single-point incremental forming of steel/steel bi-layer sheet metal. *Arch Civ Mech Eng* 20. <https://doi.org/10.1007/s43452-020-00025-1>
  55. Hassan M, Hussain G, Ali A, Ilyas M, Malik S, Khan WA, Bal B (2021) Effect of pre-rolling temperature on the interfacial properties and formability of steel-steel bilayer sheet in single point incremental forming. *P I Mech Eng B-J Eng* 235:406–416. <https://doi.org/10.1177/0954405420963004>
  56. Ashouri R, Shahrajabian H (2017) Experimental investigation of incremental forming process of bilayer hybrid brass/St13 sheets. *Int J Adv Des Manuf Technol* 3:127–135
  57. Wei H, Hussain G, Iqbal A, Zhang ZP (2019) Surface roughness as the function of friction indicator and an important parameters-combination having controlling influence on the roughness: recent results in incremental forming. *Int J Adv Manuf Technol* 101:2533–2545. <https://doi.org/10.1007/s00170-018-3096-1>
  58. Al-Ghamdi KA, Hussain G (2016) On the comparison of formability of roll-bonded steel–Cu composite sheet metal in incremental forming and stamping processes. *Int J Adv Manuf Technol* 87:267–278. <https://doi.org/10.1007/s00170-016-8488-5>
  59. Al-Ghamdi KA, Hussain G (2017) Stress gradient due to incremental forming of bonded metallic laminates. *Mater Manuf Process* 32:1384–1390. <https://doi.org/10.1080/10426914.2017.1339315>
  60. Al-Ghamdi KA, Hussain G (2016) SPIF of Cu/steel clad sheet: annealing effect on bond force and formability. *Mater Manuf Process* 31:758–763. <https://doi.org/10.1080/10426914.2015.1048363>
  61. Al-Ghamdi KA, Hussain G (2016) Parameter-formability relationship in ISF of tri-layered Cu–steel–Cu composite sheet metal: response surface and microscopic analyses. *Int J Precis Eng Man* 17:1633–1642. <https://doi.org/10.1007/s12541-016-0189-3>
  62. Al-Ghamdi KA, Hussain G (2019) Bulging in incremental sheet forming of cold bonded multi-layered Cu clad sheet: influence of forming conditions and bending. *T Nonferr Metal Soc* 29:112–122. [https://doi.org/10.1016/S1003-6326\(18\)64920-9](https://doi.org/10.1016/S1003-6326(18)64920-9)
  63. Al-Ghamdi KA, Hussain G (2019) On the free-surface roughness in incremental forming of a sheet metal: a study from the



- perspective of ISF strain, surface morphology, postforming properties, and process conditions. *Metals*
64. Shi X, Hussain G, Butt SI, Song F, Huang D, Liu Y (2017) The state of residual stresses in the Cu/steel bonded laminates after ISF deformation: an experimental analysis. *J Manuf Processes* 30:14–26. <https://doi.org/10.1016/j.jmapro.2017.09.009>
  65. Wei H, Hussain G (2019) Mechanical characteristics of a roll-bonded Cu-clad steel sheet processed through incremental forming. *Metall Mater Trans A* 50:4594–4607. <https://doi.org/10.1007/s11661-019-05366-y>
  66. Hussain G, Al-Ghamdi KA (2017) Empirical modeling and simultaneous optimization of energy efficiency/demand, cost and productivity in incremental forming of metallic clad composite. *Int J Hydrogen Energ* 42:20375–20385. <https://doi.org/10.1016/j.ijhydene.2017.06.044>
  67. Al-Ghamdi KA, Hussain G (2017) On the CO<sub>2</sub> characterization in incremental forming of roll bonded laminates. *J Clean Prod* 156:214–225. <https://doi.org/10.1016/j.jclepro.2017.04.047>
  68. Kaufmann J, Rabe H, Siebert N, Wolf P, Cebulla H, Odenwald S (2016) Smart carbon fiber bicycle seat post with light and sensor integration. *Procedia Engineering* 147:562–567. <https://doi.org/10.1016/j.proeng.2016.06.239>
  69. Holbery J, Houston D (2006) Natural-fiber-reinforced polymer composites in automotive applications. *JOM* 58:80–86
  70. Zhang J, Chaisombat K, He S, Wang CH (2012) Hybrid composite laminates reinforced with glass/carbon woven fabrics for lightweight load bearing structures. *Mater Design* 36:75–80. <https://doi.org/10.1016/j.matdes.2011.11.006>
  71. King RL (1989) Fibre-reinforced composites materials, manufacturing and design. *Composites* 20:172–173. [https://doi.org/10.1016/0010-4361\(89\)90651-4](https://doi.org/10.1016/0010-4361(89)90651-4)
  72. Vallittu PK, Närhi TO, Hupa L (2015) F Fiber glass–bioactive glass composite for bone replacing and bone anchoring implants. *Dent Mater* 31:371–381. <https://doi.org/10.1016/j.dental.2015.01.003>
  73. Chan Y, Lew W, Lu E, Loretz T, Lu L, Lin C, Feng S (2018) An evaluation of the biocompatibility and osseointegration of novel glass fiber reinforced composite implants: in vitro and in vivo studies. *Dent Mater* 34:470–485. <https://doi.org/10.1016/j.dental.2017.12.001>
  74. Conte R, Ambrogio G, Pulice D, Gagliardi F, Filice L (2017) Incremental sheet forming of a composite made of thermoplastic matrix and glass-fiber reinforcement. *Procedia Engineering* 207:819–824. <https://doi.org/10.1016/j.proeng.2017.10.835>
  75. Ambrogio G, Conte R, Gagliardi F, De Napoli L, Filice L, Russo P (2018) A new approach for forming polymeric composite structures. *Compos Struct* 204:445–453. <https://doi.org/10.1016/j.compstruct.2018.07.106>
  76. Al-Obaidi A, Kunke A, Kräusel V (2019) Hot single-point incremental forming of glass-fiber-reinforced polymer (PA6GF47) supported by hot air. *J Manuf Processes* 43:17–25. <https://doi.org/10.1016/j.jmapro.2019.04.036>
  77. Hou C, Su X, Peng X, Wu X, Yang D (2020) Thermal-assisted single point incremental forming of jute fabric reinforced poly(lactic acid) biocomposites. *Fiber Polym* 21:2373–2379. <https://doi.org/10.1007/s12221-020-1016-0>
  78. Torres S, Ortega R, Acosta P, Calderón E (2021) Hot incremental forming of biocomposites developed from linen fibres and a thermoplastic matrix. *J Mech Eng* 67:123–132
  79. Okada M, Kato T, Otsu M, Tanaka H, Miura T (2018) Development of optical-heating-assisted incremental forming method for carbon fiber reinforced thermoplastic sheet—forming characteristics in simple spot-forming and two-dimensional sheet-fed forming. *J Mater Process Technol* 256:145–153. <https://doi.org/10.1016/j.jmatprotec.2018.02.014>
  80. Xiao X, Kim J, Oh S, Kim Y (2021) Study on the incremental sheet forming of CFRP sheet. *Compos Part A-Appl S* 141:106209. <https://doi.org/10.1016/j.compositesa.2020.106209>
  81. Harhash M, Palkowski H (2021) Incremental sheet forming of steel/polymer/steel sandwich composites. *J Mater Res Technol*. <https://doi.org/10.1016/j.jmrt.2021.04.088>
  82. Jackson KP, Allwood JM, Landert M (2008) Incremental forming of sandwich panels. *J Mater Process Technol* 204:290–303. <https://doi.org/10.1016/j.jmatprotec.2007.11.117>
  83. Girjeb C, Racz G (2017) Study of the formability of laminated lightweight metallic materials. *MATEC Web of Conferences* 121. <https://doi.org/10.1051/mateconf/2017121210>
  84. Liu Z, Chen H (2020) Deformation mechanism and failure-tolerant characteristics of polymer-coated sheet metal laminates subjected to different loading conditions. *J Mater Res Technol* 9:3907–3923. <https://doi.org/10.1016/j.jmrt.2020.02.017>
  85. Davarpanah MA, Malhotra R (2018) Formability and failure modes in single point incremental forming of metal-polymer laminates. *Procedia Manufacturing* 26:343–348. <https://doi.org/10.1016/j.promfg.2018.07.042>
  86. Walczyk DF, Hosford JF, Papazian JM (2003) Using reconfigurable tooling and surface heating for incremental forming of composite aircraft parts. *J Manuf Sci E-T ASME* 125:333–343
  87. Al-Obaidi A, Graf A, Kräusel V, Trautmann M (2019) Heat supported single point incremental forming of hybrid laminates for orthopedic applications. *Procedia Manufacturing* 29:21–27. <https://doi.org/10.1016/j.promfg.2019.02.101>
  88. Gatea S, Chen F, Long H, Ou H (2017) Deformation and fracture of AMC under different heat treatment conditions and its suitability for incremental sheet forming. *Procedia Engineering* 207:848–853. <https://doi.org/10.1016/j.proeng.2017.10.840>
  89. Clavijo-Chaparro SL, Iturbe-Ek J, Lozano-Sánchez LM, Sustaita AO, Elías-Zúñiga A (2018) Plasticized and reinforced poly(methyl methacrylate) obtained by a dissolution-dispersion process for single point incremental forming: enhanced formability towards the fabrication of cranial implants. *Polym Test* 68:39–45. <https://doi.org/10.1016/j.polymertesting.2018.03.034>
  90. Borić A, Kalendová A, Urbanek M, Pepelnjak T (2019) Characterisation of polyamide (PA)12 nanocomposites with montmorillonite (MMT) filler clay used for the incremental forming of sheets. *Polymers-Basel* 11:1248. <https://doi.org/10.3390/polym11081248>
  91. Matsumoto R, Sakaguchi H, Otsu M, Utsunomiya H (2020) Plastic joining of open-cell nickel foam and polymethyl methacrylate (PMMA) sheet by friction stir incremental forming. *J Mater Process Technol* 282:116691. <https://doi.org/10.1016/j.jmatprotec.2020.116691>
  92. Lozano-Sánchez LM, Sustaita AO, Soto M, Biradar S, Ge L, Segura-Cárdenas E, Diabb J, Elizalde LE, Barrera EV, Elías-Zúñiga A (2017) Mechanical and structural studies on single point incremental forming of polypropylene-MWCNTs composite sheets. *J Mater Process Technol* 242:218–227. <https://doi.org/10.1016/j.jmatprotec.2016.11.032>
  93. Duflou JR, Habraken A, Cao J, Malhotra R, Bambach M, Adams D, Vanhove H, Mohammadi A, Jeswiet J (2018) Single point incremental forming: state-of-the-art and prospects. *Int J Mater Form* 11:743–773. <https://doi.org/10.1007/s12289-017-1387-y>
  94. Martins PAF, Bay N, Skjoedt M, Silva MB (2008) Theory of single point incremental forming. *CIRP Ann* 57:247–252. <https://doi.org/10.1016/j.cirp.2008.03.047>
  95. Silva MB, Skjoedt M, Martins PAF, Bay N (2008) Revisiting the fundamentals of single point incremental forming by means of membrane analysis. *Int J Mach Tool Manuf* 48:73–83. <https://doi.org/10.1016/j.ijmactools.2007.07.004>
  96. Silva MB, Skjoedt M, Atkins AG, Bay N, Martins PAF (2008) Single-point incremental forming and formability—failure

- diagrams. *J Strain Anal Eng* 43:15–35. <https://doi.org/10.1243/03093247JSA340>
97. Allwood JM, Shouler DR, Tekkaya AE (2007) The increased forming limits of incremental sheet forming processes. *Key Eng Mater* 344:621–628
  98. Jackson K, Allwood J (2009) The mechanics of incremental sheet forming. *J Mater Process Technol* 209:1158–1174
  99. Malhotra R, Xue L, Belytschko T, Cao J (2012) Mechanics of fracture in single point incremental forming. *J Mater Process Technol* 212:1573–1590. <https://doi.org/10.1016/j.jmatprotec.2012.02.021>
  100. Smith J, Malhotra R, Liu WK, Cao J (2013) Deformation mechanics in single-point and accumulative double-sided incremental forming. *Int J Adv Manuf Technol* 69:1185–1201. <https://doi.org/10.1007/s00170-013-5053-3>
  101. Lu B, Fang Y, Xu DK, Chen J, Ou H, Moser NH, Cao J (2014) Mechanism investigation of friction-related effects in single point incremental forming using a developed oblique roller-ball tool. *Int J Mach Tool Manuf* 85:14–29. <https://doi.org/10.1016/j.ijmactools.2014.04.007>
  102. Emmens WC, van den Boogaard AH (2008) Tensile tests with bending: a mechanism for incremental forming. *Int J Mater Form* 1:1155–1158. <https://doi.org/10.1007/s12289-008-0185-y>
  103. Emmens WC, van den Boogaard AH (2009) An overview of stabilizing deformation mechanisms in incremental sheet forming. *J Mater Process Technol* 209:3688–3695. <https://doi.org/10.1016/j.jmatprotec.2008.10.003>
  104. Fang Y, Lu B, Chen J, Xu DK, Ou H (2014) Analytical and experimental investigations on deformation mechanism and fracture behavior in single point incremental forming. *J Mater Process Technol* 214:1503–1515. <https://doi.org/10.1016/j.jmatprotec.2014.02.019>
  105. Franzen V, Kwiatkowski L, Martins PAF, Tekkaya AE (2009) Single point incremental forming of PVC. *J Mater Process Technol* 209:462–469. <https://doi.org/10.1016/j.jmatprotec.2008.02.013>
  106. Yang Z, Chen F (2020) Mechanism of twist in incremental sheet forming of thermoplastic polymer. *Mater Des* 195:108997. <https://doi.org/10.1016/j.matdes.2020.108997>
  107. Do V, Pham Q, Kim Y (2017) Identification of forming limit curve at fracture in incremental sheet forming. *Int J Adv Manuf Technol* 92:4445–4455. <https://doi.org/10.1007/s00170-017-0441-8>
  108. Mirnia MJ, Shamsari M (2017) Numerical prediction of failure in single point incremental forming using a phenomenological ductile fracture criterion. *J Mater Process Technol* 244:17–43. <https://doi.org/10.1016/j.jmatprotec.2017.01.029>
  109. Shi P, Li Y, Yang M (2018) Formation and laws of convex on single-point thermal incremental forming part. *Int J Performability Eng* 12:3247–3256
  110. Liu X, Huang L, Li J, Su H (2019) Electromagnetic incremental forming (EMIF) strategy for large-scale parts of aluminum alloy based on dual coil. *Int J Adv Manuf Technol* 104:411–431. <https://doi.org/10.1007/s00170-019-03892-y>
  111. Hussain G, Valaei H, Al-Ghamdi KA, Khan B (2016) Finite element and experimental analyses of cylindrical hole flanging in incremental forming. *T Nonferrous Metal Soc* 26:2419–2425. [https://doi.org/10.1016/S1003-6326\(16\)64362-5](https://doi.org/10.1016/S1003-6326(16)64362-5)
  112. Isidore BBL, Hussain G, Shamchi SP, Khan WA (2016) Prediction and control of pillow defect in single point incremental forming using numerical simulations. *J Mech Sci Technol* 30:2151–2161. <https://doi.org/10.1007/s12206-016-0422-0>
  113. Lingam R, Lingam R, Bansal A, Bansal A, Reddy NV, Reddy NV (2016) Analytical prediction of formed geometry in multi-stage single point incremental forming. *Int J Mater Form* 9:395–404. <https://doi.org/10.1007/s12289-015-1226-y>
  114. Bansal A, Lingam R, Yadav SK, Venkata Reddy N (2017) Prediction of forming forces in single point incremental forming. *J Manuf Process* 28:486–493. <https://doi.org/10.1016/j.jmapro.2017.04.016>
  115. Mugendiran V, Gnanavelbabu A (2017) Comparison of plastic strains on AA5052 by single point incremental forming process using digital image processing. *J Mech Sci Technol* 31:2943–2949. <https://doi.org/10.1007/s12206-017-0537-y>
  116. Nirala HK, Jain PK, Roy JJ, Samal MK, Tandon P (2017) An approach to eliminate stepped features in multistage incremental sheet forming process: experimental and FEA analysis. *J Mech Sci Technol* 31:599–604. <https://doi.org/10.1007/s12206-017-0112-6>
  117. Raju C, Haloi N, Sathiya Narayanan C (2017) Strain distribution and failure mode in single point incremental forming (SPIF) of multiple commercially pure aluminum sheets. *J Manuf Process* 30:328–335. <https://doi.org/10.1016/j.jmapro.2017.09.033>
  118. Gupta P, Jeswiet J (2018) Effect of temperatures during forming in single point incremental forming. *Int J Adv Manuf Technol* 95:3693–3706
  119. Besong LI, Buhl J, Bambach M (2019) Investigations on hole-flanging by paddle forming and a comparison with single point incremental forming. *Int J Mech Sci* 164:105143. <https://doi.org/10.1016/j.ijmecsci.2019.105143>
  120. Choi H, Lee C (2019) A Mathematical model to predict thickness distribution and formability of incremental forming combined with stretch forming. *Robot Cim-Int Manuf* 55:164–172. <https://doi.org/10.1016/j.rcim.2018.07.014>
  121. Guo X, Wang C, Xu Y, El-Aty AA, Zhang S (2019) Incremental forming characteristics of hollow parts with grooves. *Int J Adv Manuf Technol* 102:829–837. <https://doi.org/10.1007/s00170-018-3201-5>
  122. Gupta P, Szekeres A, Jeswiet J (2019) Design and development of an aerospace component with single-point incremental forming. *Int J Adv Manuf Technol* 103:3683–3702. <https://doi.org/10.1007/s00170-019-03622-4>
  123. Kumar A, Gulati V, Kumar P, Singh V, Kumar B, Singh H (2019) Parametric effects on formability of AA2024-O aluminum alloy sheets in single point incremental forming. *J Mater Res Technol* 8:1461–1469. <https://doi.org/10.1016/j.jmrt.2018.11.001>
  124. Buffa G, Gucciardi M, Fratini L, Micari F (2020) Multi-directional vs. mono-directional multi-step strategies for single point incremental forming of non-axisymmetric components. *J Manuf Process* 55:22–30. <https://doi.org/10.1016/j.jmapro.2020.03.055>
  125. Su C, Zhao Z, Lv Y, Wang R, Wang Q, Wang M (2019) Effect of process parameters on plastic formability and microstructures of magnesium alloy in single point incremental forming. *J Mater Eng Perform* 28:7737–7755. <https://doi.org/10.1007/s11665-019-04460-x>
  126. de Castro Maciel D, Silva GCD, de Quadros LM (2020) Incremental stamping forming with use of roller ball tool in aluminum and magnesium alloy. *Int J Adv Manuf Technol* 108:455–462. <https://doi.org/10.1007/s00170-020-05425-4>
  127. Luo Y, Luo Y, Yang W, Yang W, Liu Z, Liu Z, Wang Y, Wang Y, Du R, Du R (2016) Numerical simulation and experimental study on cyclic multi-point incremental forming process. *Int J Adv Manuf Technol* 85:1249–1259. <https://doi.org/10.1007/s00170-015-8030-1>
  128. Fiorentino A, Fiorentino A, Feriti GC, Feriti GC, Ceretti E, Ceretti E, Giardini C, Giardini C (2018) Capability of iterative learning control and influence of the material properties on the improvement of the geometrical accuracy in incremental sheet forming process. *Int J Mater Form* 11:125–134. <https://doi.org/10.1007/s12289-016-1335-2>
  129. Teymoori F, Lohmousavi M, Etesam A (2016) Numerical analysis of fluid structure interaction in water jet incremental sheet

- forming process using coupled Eulerian-Lagrangian approach. *Int J Interact Des Manuf* 10:203–210. <https://doi.org/10.1007/s12008-013-0197-9>
130. Li Y, Daniel WJT, Meehan PA (2017) Deformation analysis in single-point incremental forming through finite element simulation. *Int J Adv Manuf Technol* 88:255–267. <https://doi.org/10.1007/s00170-016-8727-9>
  131. Long Y, Li Y, Sun J, Ille I, Li J, Twiefel J (2018) Effects of process parameters on force reduction and temperature variation during ultrasonic assisted incremental sheet forming process. *Int J Adv Manuf Technol* 97:13–24. <https://doi.org/10.1007/s00170-018-1886-0>
  132. Perez-Santiago R, Bagudanch I, García-Romeu ML, Nicolas H (2012) Effect of strain hardening exponent in the incremental sheet forming force. *Proc. 14th Int. Conf. Metal Forming*
  133. Centeno G, Bagudanch I, Martínez-Donaire AJ, García-Romeu ML, Vallengano C (2014) Critical analysis of necking and fracture limit strains and forming forces in single-point incremental forming. *Mater Des* 63:20–29. <https://doi.org/10.1016/j.matdes.2014.05.066>
  134. Nguyen D, Park J, Kim Y (2010) Ductile fracture prediction in rotational incremental forming for magnesium alloy sheets using combined kinematic/isotropic hardening model. *Metall Mater Trans A Phys Metall Mater Sci* 41:1983–1994. <https://doi.org/10.1007/s11661-010-0235-1>
  135. Shamsari M, Shamsari M, Mirnia MJ, Mirnia MJ, Elyasi M, Elyasi M, Baseri H, Baseri H, Liu C, Li Y et al (2018) Formability improvement in single point incremental forming of truncated cone using a two-stage hybrid deformation strategy. *Int J Adv Manuf Technol* 94:2357–2368. <https://doi.org/10.1007/s00170-017-1031-5>
  136. Nourmohammadi AA, Elyasi M, Mirnia MJ (2019) Flexibility improvement in two-point incremental forming by implementing multi-point die. *Int J Adv Manuf Technol* 102:2933–2952. <https://doi.org/10.1007/s00170-019-03307-y>
  137. Ai S, Dai R, Long H (2020) Investigating formability enhancement in double side incremental forming by developing a new test method of tension under cyclic bending and compression. *J Mater Process Technol* 275:116349. <https://doi.org/10.1016/j.jmatprotec.2019.116349>
  138. Shi Y, Zhang W, Cao J, Ehmann KF (2019) An experimental and numerical study of dieless water jet incremental micro-forming. *J Manuf Sci E- T ASME* 141
  139. Wen T, Zhang S, Zheng J, Huang Q, Liu Q (2016) Bi-directional dieless incremental flanging of sheet metals using a bar tool with tapered shoulders. *J Mater Process Technol* 229:795–803. <https://doi.org/10.1016/j.jmatprotec.2015.11.005>
  140. Movahedinia H, Movahedinia H, Mirnia MJ, Mirnia MJ, Elyasi M, Elyasi M, Baseri H, Baseri H (2018) An investigation on flaring process of thin-walled tubes using multistage single point incremental forming. *Int J Adv Manuf Technol* 94:867–880. <https://doi.org/10.1007/s00170-017-0971-0>
  141. Zhiheng W, Xuepeng Z, Jun C (2020) An effective thermal-mechanical coupling method for simulating friction stir-assisted incremental aluminum alloy sheet forming. *Int J Adv Manuf Technol* 107:3449–3458. <https://doi.org/10.1007/s00170-020-05286-x>
  142. Zhang H, Lu B, Chen J, Feng S, Li Z, Long H (2017) Thickness control in a new flexible hybrid incremental sheet forming process. *P I Mech Eng B-J Eng* 231:779–791. <https://doi.org/10.1177/0954405417694061>
  143. Benedetti M, Fontanari V, Monelli B, Tassan M (2017) Single-point incremental forming of sheet metals: experimental study and numerical simulation. *P I Mech Eng B-J Eng* 231:301–312. <https://doi.org/10.1177/0954405415612351>
  144. Boudhaouia S, Boudhaouia S, Gahbiche MA, Gahbiche MA, Ayed Y, Ayed Y, Giraud E, Giraud E, Ben Salem W, Ben Salem W et al (2018) Experimental and numerical study of a new hybrid process: multi-point incremental forming (MPIF). *Int J Mater Form* 11:815–827. <https://doi.org/10.1007/s12289-017-1392-1>
  145. Morales-Palma D, Borrego M, Martínez-Donaire A, Centeno G, Vallengano C (2020) Optimization of hole-flanging by single point incremental forming in two stages. *Materials* 2018:11. <https://doi.org/10.3390/ma11102029>
  146. Moser N, Pritchett D, Ren H, Ehmann KF, Cao J (2016) An efficient and general finite element model for double-sided incremental forming. *J Manuf Sci E- T ASME* 138
  147. Ren H, Moser N, Zhang Z, Ndir-Agbor E, Smith J, Ehmann KF (2015) Effects of tool positions in accumulated double-sided incremental forming on part geometry. *J Manuf Sci E- T ASME* 137
  148. Mohammadi A, Mohammadi A, Vanhove H, Vanhove H, Van Bael A, Van Bael A, Dufloy JR, Dufloy JR (2016) Towards accuracy improvement in single point incremental forming of shallow parts formed under laser assisted conditions. *Int J Mater Form* 9:339–351. <https://doi.org/10.1007/s12289-014-1203-x>
  149. Eyckens P, Del-Lero Moreau J, Dufloy JR, Van Bael A, Van Houtte P (2009) MK Modelling of sheet formability in the incremental sheet forming process, taking into account through-thickness shear. *Int J Mater Form* 2:379–382. <https://doi.org/10.1007/s12289-009-0458-0>
  150. Wang H, Zhang R, Zhang H, Hu Q, Chen J (2018) Novel strategies to reduce the springback for double-sided incremental forming. *Int J Adv Manuf Technol* 96:973–979. <https://doi.org/10.1007/s00170-018-1659-9>
  151. Robert C, Dal Santo P, Delamézière A, Potiron A, Batoz JL (2008) On some computational aspects for incremental sheet metal forming simulations. *Int J Mater Form* 1:1195–1198. <https://doi.org/10.1007/s12289-008-0155-4>
  152. Hadoush A, van den Boogaard AH (2009) On the performance of substructuring implicit simulation of single point incremental forming. *Int J Mater Form* 2:559–562. <https://doi.org/10.1007/s12289-009-0427-7>
  153. Hadoush A, van den Boogaard AH (2009) Substructuring in the implicit simulation of single point incremental sheet forming: the incrementally updated approach. *Int J Mater Form* 2:181–189. <https://doi.org/10.1007/s12289-009-0402-3>
  154. Min J, Kuhlénkötter B, Shu C, Störkle D, Thyssen L (2018) Experimental and numerical investigation on incremental sheet forming with flexible die-support from metallic foam. *J Manuf Process* 31:605–612. <https://doi.org/10.1016/j.jmapro.2017.12.013>
  155. Verbert J, Belkassen B, Henrard C, Habraken AM, Gu J, Sol H, Lauwers B, Dufloy JR (2008) Multi-step toolpath approach to overcome forming limitations in single point incremental forming. *Int J Mater Form* 1:1203–1206. <https://doi.org/10.1007/s12289-008-0157-2>
  156. Panjwani D, Priyadarshi S, Jain PK, Samal MK, Roy JJ, Roy D, Tandon P (2017) A novel approach based on flexible supports for forming non-axisymmetric parts in SPISF. *Int J Adv Manuf Technol* 92:2463–2477. <https://doi.org/10.1007/s00170-017-0223-3>
  157. Shrivastava P, Tandon P (2019) Microstructure and texture based analysis of forming behavior and deformation mechanism of AA1050 sheet during single point incremental forming. *J Mater Process Technol* 266:292–310. <https://doi.org/10.1016/j.jmatprotec.2018.11.012>
  158. Mohanraj R, Elangovan S (2020) Metal forming of Ti6Al4V alloy for aerospace application. *T Can Soc Mech Eng* 1:56–64
  159. Shrivastava P, Kumar P, Tandon P, Pesin A (2018) Improvement in formability and geometrical accuracy of incrementally



- formed AA1050 sheets by microstructure and texture reformation through preheating, and their FEA and experimental validation. *J Braz Soc Mech Sci* 40:1–15. <https://doi.org/10.1007/s40430-018-1255-9>
160. Honarpisheh M, Honarpisheh M, Abdolhoseini MJ, Abdolhoseini MJ, Amini S, Amini S (2016) Experimental and numerical investigation of the hot incremental forming of Ti-6Al-4V sheet using electrical current. *Int J Adv Manuf Technol* 83:2027–2037. <https://doi.org/10.1007/s00170-015-7717-7>
  161. Pacheco PAP, Silveira ME (2018) Numerical simulation of electric hot incremental sheet forming of 1050 aluminum with and without preheating. *Int J Adv Manuf Technol* 94:3097–3108. <https://doi.org/10.1007/s00170-017-0879-8>
  162. Pacheco PAP, Silveira ME, Silva JA (2019) Heat distribution in electric hot incremental sheet forming. *Int J Adv Manuf Technol* 102:991–998. <https://doi.org/10.1007/s00170-018-03228-2>
  163. Leitao G, Yixi Z, Zhongqi Y, Hui Y (2020) Formability analysis of electrically assisted double-side multi-point incremental sheet forming. *Int J Adv Manuf Technol* 108:3405–3417. <https://doi.org/10.1007/s00170-020-05576-4>
  164. Zheng C, Pan C, Tian Z, Zhao X, Zhao G, Ji Z, Song L (2020) Laser shock induced incremental forming of pure copper foil and its deformation behavior. *Opt Laser Technol* 121:105785. <https://doi.org/10.1016/j.optlastec.2019.105785>
  165. Zheng C, Tian Z, Zhao X, Tan Y, Zhang G, Zhao G, Ji Z (2020) Effect of pulsed laser parameters on deformation inhomogeneity in laser shock incremental forming of pure copper foil. *Opt Laser Technol* 127:106205. <https://doi.org/10.1016/j.optlastec.2020.106205>
  166. Henrard C, Henrard C, Bouffioux C, Bouffioux C, Eyckens P, Eyckens P, Sol H, Sol H, Dufflou JR, Dufflou JR et al (2011) Forming forces in single point incremental forming: prediction by finite element simulations, validation and sensitivity. *Comput Mech* 47:573–590. <https://doi.org/10.1007/s00466-010-0563-4>
  167. Esmaeilpour R, Kim H, Park T, Pourboghra F, Mohammed B (2017) Comparison of 3D yield functions for finite element simulation of single point incremental forming (SPIF) of aluminum 7075. *Int J Mech Sci* 133:544–554. <https://doi.org/10.1016/j.ijmecsci.2017.09.019>
  168. Han K, Li X, Peng X, Wang H, Li D, Li Y, Li Q (2019) Experimental and numerical study on the deformation mechanism of straight flanging by incremental sheet forming. *Int J Mech Sci* 160:75–89. <https://doi.org/10.1016/j.ijmecsci.2019.06.024>
  169. Said LB, Mars J, Wali M, Dammak F (2017) Numerical prediction of the ductile damage in single point incremental forming process. *Int J Mech Sci* 131–132:546–558. <https://doi.org/10.1016/j.ijmecsci.2017.08.026>
  170. Jin K, Guo X, Tao J, Wang H, Kim N, Gu Y (2016) A model of one-surface cyclic plasticity with lemaître damage criterion for plastic instability prediction in the incremental forming process. *Int J Mech Sci* 114:88–97. <https://doi.org/10.1016/j.ijmecsci.2016.05.016>
  171. Basak S, Prasad KS, Sidpara AM, Panda SK (2019) Single point incremental forming of AA6061 thin sheet: calibration of ductile fracture models incorporating anisotropy and post forming analyses. *Int J Mater Form* 12:623–642. <https://doi.org/10.1007/s12289-018-1439-y>
  172. Gatea S, Lu B, Chen J, Ou H, McCartney G (2019) Investigation of the effect of forming parameters in incremental sheet forming using a micromechanics based damage model. *Int J Mater Form* 12:553–574. <https://doi.org/10.1007/s12289-018-1434-3>
  173. Gatea S, Gatea S, Xu D, Xu D, Ou H, Ou H, McCartney G, McCartney G (2018) Evaluation of formability and fracture of pure titanium in incremental sheet forming. *Int J Adv Manuf Technol* 95:625–641. <https://doi.org/10.1007/s00170-017-1195-z>
  174. Guzmán CF, Yuan S, Duchêne L, Saavedra Flores EI, Habraken AM (2018) Damage prediction in single point incremental forming using an extended Gurson model. *Int J Solids Struct* 151:45–56. <https://doi.org/10.1016/j.ijsolstr.2017.04.013>
  175. Marathe SP, Raval HK (2019) Numerical investigation on forming behavior of friction stir tailor welded blanks (FSTWBs) during single-point incremental forming (SPIF) process. *J Braz Soc Mech Sci* 41:1–18. <https://doi.org/10.1007/s40430-019-1929-y>
  176. Renhao W, Meng L, Sheng C, Xinmei L, Mei Y, Wenshuai H, Jun C (2020) Analytical model for temperature prediction in friction stir-assisted incremental forming with synchronous bonding of dissimilar sheet metals. *Int J Adv Manuf Technol* 107:2177–2187. <https://doi.org/10.1007/s00170-020-05144-w>
  177. Liu K, Zhang B, Xu X, Ye J, Liu C (2019) Simulation and analysis of process-induced distortions in hemispherical thermostamping for unidirectional thermoplastic composites. *Polym Composite* 40:1786–1800. <https://doi.org/10.1002/pc.24936>
  178. Venkatesan S, Kalyanasundaram S (2010) Finite element analysis and optimization of process parameters during stamp forming of composite materials. *IOP Conf Ser Mater Sci Eng* 10:12138. <https://doi.org/10.1088/1757-899X/10/1/012138>
  179. Tang H, Dai H, Wu H (2021) An effect of hygrothermal effects on high velocity impact event for polymer matrix composites. *Appl Math Model* 91:653–669. <https://doi.org/10.1016/j.apm.2020.09.062>
  180. Uscinowicz R (2013) Experimental identification of yield surface of Al–Cu bimetallic sheet. *Compos Part B-Eng* 55:96–108. <https://doi.org/10.1016/j.compositesb.2013.06.002>
  181. Wang Z, Zhang W, Luo Q, Zheng G, Li Q, Sun G (2020) A novel failure criterion based upon forming limit curve for thermoplastic composites. *Compos Part B-Eng* 202:108320. <https://doi.org/10.1016/j.compositesb.2020.108320>
  182. Kazemi ME, Shanmugam L, Dadashi A, Shakouri M, Lu D, Du Z, Hu Y, Wang J, Zhang W, Yang L et al (2021) Investigating the roles of fiber, resin, and stacking sequence on the low-velocity impact response of novel hybrid thermoplastic composites. *Compos Part B-Eng* 207:108554. <https://doi.org/10.1016/j.compositesb.2020.108554>
  183. Zhang J, Zhang X (2015) Simulating low-velocity impact induced delamination in composites by a quasi-static load model with surface-based cohesive contact. *Compos Struct* 125:51–57. <https://doi.org/10.1016/j.compstruct.2015.01.050>
  184. Fu T, Xu J, Hui Z (2021) Analysis of induction heating temperature field of plain weave CFRP based on finite element meso model. *Appl Compos Mater* 28:149–163. <https://doi.org/10.1007/s10443-020-09852-0>
  185. Centeno G, Bagudanch I, Martínez-Donaire AJ, García-Romeu ML, Vallellano C (2014) Critical analysis of necking and fracture limit strains and forming forces in single point incremental forming. *Mater Design*
  186. Isik K, Silva MB, Tekkaya AE, Martins PAF (2014) Formability limits by fracture in sheet metal forming. *J Mater Process Technol* 214:1557–1565. <https://doi.org/10.1016/j.jmatprotec.2014.02.026>
  187. Silva MB, Nielsen PS, Bay N, Martins PAF (2011) Failure mechanisms in single-point incremental forming of metals. *Int J Adv Manuf Technol* 56:893–903. <https://doi.org/10.1007/s00170-011-3254-1>
  188. Liu Z, Li Y, Meehan PA (2013) Experimental investigation of mechanical properties, formability and force measurement for AA7075-O aluminium alloy sheets formed by incremental forming. *Int J Precis Eng Man* 11:1891–1899
  189. Li P, He J, Liu Q, Yang M, Wang Q, Yuan Q, Li Y (2017) Evaluation of forming forces in ultrasonic incremental sheet metal forming. *Aerosp Sci Technol* 63:132–139. <https://doi.org/10.1016/j.ast.2016.12.028>



190. Bai L, Li Y, Yang M, Yao Z, Yao Z, Kou H (2018) Influences of process parameters and vibration parameters on the forming force in the ultrasonic-assisted incremental forming process. *Adv Mater Sci Eng* 2018:1–12. <https://doi.org/10.1155/2018/5726845>
191. Kumar A, Gulati V (2018) Experimental investigations and optimization of forming force in incremental sheet forming. *Sadhana-Acad P Eng S* 43:1–15. <https://doi.org/10.1007/s12046-018-0926-7>
192. Ren H, Li F, Moser N, Leem D, Li T, Ehmann K, Cao J (2018) General contact force control algorithm in double-sided incremental forming. *CIRP Ann* 67:381–384. <https://doi.org/10.1016/j.cirp.2018.04.057>
193. Bai L, Li Y, Yang M, Lin Y, Yuan Q, Zhao R (2019) Modeling and analysis of single point incremental forming force with static pressure support and ultrasonic vibration. *Materials* 12. <https://doi.org/10.3390/ma12121899>
194. Chang Z, Li M, Chen J (2019) Analytical modeling and experimental validation of the forming force in several typical incremental sheet forming processes. *Int J Mach Tool Manuf* 140:62–76. <https://doi.org/10.1016/j.ijmactools.2019.03.003>
195. Kumar A, Gulati V, Kumar P, Singh H (2019) Forming force in incremental sheet forming: a comparative analysis of the state of the art. *J Braz Soc Mech Sci* 41:1–45. <https://doi.org/10.1007/s40430-019-1755-2>
196. Torsakul S, Kuptasthien N (2019) Effects of three parameters on forming force of the single point incremental forming process. *J Mech Sci Technol* 33:2817–2823. <https://doi.org/10.1007/s12206-019-0528-2>
197. Xiao X, Kim C, Lv X, Hwang T, Kim Y (2019) Formability and forming force in incremental sheet forming of AA7075-T6 at different temperatures. *J Mech Sci Technol* 33:3795–3802. <https://doi.org/10.1007/s12206-019-0722-2>
198. Kilani L, Mabrouki T, Ayadi M, Chermiti H, Belhadi S (2020) Effects of rolling ball tool parameters on roughness, sheet thinning, and forming force generated during SPIF process. *Int J Adv Manuf Technol* 106:4123–4142. <https://doi.org/10.1007/s00170-019-04918-1>
199. Zhai W, Li Y, Cheng Z, Sun L, Li F, Li J (2020) Investigation on the forming force and surface quality during ultrasonic-assisted incremental sheet forming process. *Int J Adv Manuf Technol* 106:2703–2719. <https://doi.org/10.1007/s00170-019-04870-0>
200. Al-Ghamdi KA, Hussain G (2015) Forming forces in incremental forming of a geometry with corner feature: investigation into the effect of forming parameters using response surface approach. *Int J Adv Manuf Technol* 76:2185–2197. <https://doi.org/10.1007/s00170-014-6409-z>
201. Liu Z, Li Y (2020) Small data-driven modeling of forming force in single point incremental forming using neural networks. *Eng Comput-Germany* 36:1589–1597. <https://doi.org/10.1007/s00366-019-00781-6>
202. Bagudanch I, Garcia-Romeu ML, Centeno G, El Iaszu Niga A, Ciurana J (2014) Forming force and temperature effects on single point incremental forming of polyvinylchloride. *J Mater Process Technol*
203. Li Y, Liu Z, Lu H, Daniel WJT, Liu S, Meehan PA (2014) Efficient force prediction for incremental sheet forming and experimental validation. *Int J Adv Manuf Technol* 73:571–587. <https://doi.org/10.1007/s00170-014-5665-2>
204. Behera AK, Ou H (2016) Effect of stress relieving heat treatment on surface topography and dimensional accuracy of incrementally formed grade 1 titanium sheet parts. *Int J Adv Manuf Technol* 87:3233–3248. <https://doi.org/10.1007/s00170-016-8610-8>
205. Behera AK, Lu B, Ou H (2016) Characterization of shape and dimensional accuracy of incrementally formed titanium sheet parts with intermediate curvatures between two feature types. *Int J Adv Manuf Technol* 83:1099–1111. <https://doi.org/10.1007/s00170-015-7649-2>
206. Lu H, Kearney M, Li Y, Liu S, Daniel WJT, Meehan PA (2016) Model predictive control of incremental sheet forming for geometric accuracy improvement. *Int J Adv Manuf Technol* 82:1781–1794. <https://doi.org/10.1007/s00170-015-7431-5>
207. Rakesh L, Amit S, Reddy NV (2016) Deflection compensations for tool path to enhance accuracy during double-sided incremental forming. *J Manuf Sci Eng Trans ASME* 138
208. Li L, Wang J, Wang B (2017) Geometric accuracy of incremental sheet forming for TRIP590. *J Mech Sci Technol* 31:5257–5264. <https://doi.org/10.1007/s12206-017-1018-z>
209. Li Z, Lu S, Zhang T, Mao Z, Zhang C (2017) Analysis of geometrical accuracy based on multistage single point incremental forming of a straight wall box part. *Int J Adv Manuf Technol* 93:2783–2789. <https://doi.org/10.1007/s00170-017-0723-1>
210. Lingam R, Prakash O, Belk JH, Reddy NV (2017) Automatic feature recognition and tool path strategies for enhancing accuracy in double sided incremental forming. *Int J Adv Manuf Technol* 88:1639–1655. <https://doi.org/10.1007/s00170-016-8880-1>
211. Mohammadi A, Vanhove H, Van Bael A, Seefeldt M, Seefeldt M (2017) Effect of laser transformation hardening on the accuracy of SPIF formed parts. *J Manuf Sci E- T ASME* 139
212. Khan S, Hussain G, Ilyas M, Rashid H, Khan MI, Khan WA (2018) Appropriate heat treatment and incremental forming route to produce age-hardened components of Al-2219 alloy with minimized form error and high formability. *J Mater Process Technol* 256:262–273. <https://doi.org/10.1016/j.jmatprotec.2017.12.042>
213. Maqbool F, Bambach M (2018) Dominant deformation mechanisms in single point incremental forming (SPIF) and their effect on geometrical accuracy. *Int J Mech Sci* 136:279–292. <https://doi.org/10.1016/j.ijmecsci.2017.12.053>
214. Mingshun Y, Lang B, Yunbo L, Yan L, Qilong Y, Renfeng Z (2019) Research on the radial accuracy of ultrasonic vibration-assisted single point incremental forming parts. *Int J Aerospace Eng* 2019:1–9. <https://doi.org/10.1155/2019/9809815>
215. Dabwan A, Ragab AE, Saleh MA, Anwar S, Ghaleb AM, Rehman AU (2020) Study of the effect of process parameters on surface profile accuracy in single-point incremental sheet forming of AA1050-H14 aluminum alloy. *Adv Mater Sci Eng* 2020:1–14. <https://doi.org/10.1155/2020/7265941>
216. Sbayit M, Bahloul R, Belhadjsalah H (2020) Efficiency of optimization algorithms on the adjustment of process parameters for geometric accuracy enhancement of denture plate in single point incremental sheet forming. *Neural Comput Appl* 32:8829–8846. <https://doi.org/10.1007/s00521-019-04354-y>
217. Zhang Z, Ren H, Xu R, Moser N, Smith J, Ndip-Agbor E, Malhotra R, Xia ZC, Cao J (2015) A mixed double-sided incremental forming toolpath strategy for improved geometric accuracy. *J Manuf Sci E- T ASME* 137
218. Shi X, Gao L, Khalatbari H, Xu Y, Wang H, Jin L (2013) Electric hot incremental forming of low carbon steel sheet: accuracy improvement. *Int J Adv Manuf Technol* 68:241–247. <https://doi.org/10.1007/s00170-013-4724-4>
219. Voswinkel H, Bambach M, Hirt G (2015) Improving geometrical accuracy for flanging by incremental sheet metal forming. *Int J Mater Form* 8:391–399. <https://doi.org/10.1007/s12289-014-1182-y>
220. Li Y, Lu H, Daniel WJT, Meehan PA (2015) Investigation and optimization of deformation energy and geometric accuracy in the incremental sheet forming process using response surface methodology. *Int J Adv Manuf Technol* 79:2041–2055. <https://doi.org/10.1007/s00170-015-6986-5>
221. Najafabady SA, Ghaei A (2016) An experimental study on dimensional accuracy, surface quality, and hardness of Ti-6Al-4 V titanium alloy sheet in hot incremental forming. *Int*

- J Adv Manuf Technol 87:3579–3588. <https://doi.org/10.1007/s00170-016-8712-3>
222. Formisano A, Durante M, Boccarusso L, Astarita A (2017) The influence of thermal oxidation and tool-sheet contact conditions on the formability and the surface quality of incrementally formed grade 1 titanium thin sheets. *Int J Adv Manuf Technol* 93:3723–3732. <https://doi.org/10.1007/s00170-017-0805-0>
  223. Mulay A, Ben S, Ismail S, Kocanda A (2017) Experimental investigations into the effects of SPIF forming conditions on surface roughness and formability by design of experiments. *J Braz Soc Mech Sci* 39:3997–4010. <https://doi.org/10.1007/s40430-016-0703-7>
  224. Mohanty S, Regalla SP, Daseswara Rao YV (2018) Investigation of influence of part inclination and rotation on surface quality in robot assisted incremental sheet metal forming (RAISF). *CIRP J Manuf Sci Technol* 22:37–48. <https://doi.org/10.1016/j.cirpj.2018.04.005>
  225. Ramkumar K, Paulraj G, Elangovan K, Sathiyaraj Narayanan C (2018) Forming limit diagram, void analysis, strain distribution and surface roughness for SS430 sheets during multipoint incremental forming. *Arch Metall Mater* 63:1709–1714. <https://doi.org/10.24425/amm.2018.125096>
  226. Chang Z, Chen J (2019) Analytical model and experimental validation of surface roughness for incremental sheet metal forming parts. *Int J Mach Tool Manuf* 146:103453. <https://doi.org/10.1016/j.ijmactools.2019.103453>
  227. Dakhli M, Boulila A, Manach P, Tourki Z (2019) Optimization of processing parameters and surface roughness of metallic sheets plastically deformed by incremental forming process. *Int J Adv Manuf Technol* 102:977–990. <https://doi.org/10.1007/s00170-018-03265-x>
  228. Kumar A, Gulati V (2019) Experimental investigation and optimization of surface roughness in negative incremental forming. *Measurement* 131:419–430. <https://doi.org/10.1016/j.measurement.2018.08.078>
  229. Mulay A, Ben BS, Ismail S, Kocanda A (2019) Prediction of average surface roughness and formability in single point incremental forming using artificial neural network. *Arch Civ Mech Eng* 19:1135–1149. <https://doi.org/10.1016/j.acme.2019.06.004>
  230. Gandla PK, Inturi V, Kurra S, Radhika S (2020) Evaluation of surface roughness in incremental forming using image processing based methods. *Measurement* 164:108055. <https://doi.org/10.1016/j.measurement.2020.108055>
  231. Taherkhani A, Basti A, Nariman-Zadeh N, Jamali A (2019) Achieving maximum dimensional accuracy and surface quality at the shortest possible time in single-point incremental forming via multi-objective optimization. *P I Mech Eng B-J Eng* 233:900–913. <https://doi.org/10.1177/0954405418755822>
  232. Wang Z, Cai S, Chen J (2020) Experimental investigations on friction stir assisted single point incremental forming of low-ductility aluminum alloy sheet for higher formability with reasonable surface quality. *J Mater Process Technol* 277:116488. <https://doi.org/10.1016/j.jmatprotec.2019.116488>
  233. Bhattacharya A, Maneesh K, Reddy NV, Cao J (2011) Formability and surface finish studies in single point incremental forming. *J Manuf Sci E- T ASME* 133
  234. Kurra S, Hifzur Rahman N, Regalla SP, Gupta AK (2015) Modeling and optimization of surface roughness in single point incremental forming process. *J Mater Res Technol* 4:304–313. <https://doi.org/10.1016/j.jmrt.2015.01.003>
  235. Fiorentino A, Marzi R, Ceretti E (2012) Preliminary results on Ti incremental sheet forming (ISF) of biomedical devices: biocompatibility, surface finishing and treatment. *Int J Mechatron Manuf Syst* 5:36–45
  236. Liu Z, Liu S, Li Y, Meehan PA (2014) Modeling and optimization of surface roughness in incremental sheet forming using a multi-objective function. *Mater Manuf Process* 29:808–818. <https://doi.org/10.1080/10426914.2013.864405>
  237. Hamilton K, Jeswiet J (2010) Visual categorization and quantification of the orange peel effect in single point incremental forming at high forming speeds. *Trans NAMRI/SME* 38:679–686
  238. Echraf SBM, Hrairi M (2014) Significant parameters for the surface roughness in incremental forming process. *Mater Manuf Process* 29:697–703. <https://doi.org/10.1080/10426914.2014.901519>
  239. Radu MC, Cristea I (2013) Processing metal sheets by SPIF and analysis of parts quality. *Mater Manuf Process* 28:287–293. <https://doi.org/10.1080/10426914.2012.746702>
  240. Maji K, Kumar G (2020) Inverse analysis and multi-objective optimization of single-point incremental forming of AA5083 aluminum alloy sheet. *Soft Comput* 24:4505–4521. <https://doi.org/10.1007/s00500-019-04211-z>
  241. Milutinović M, Lendjel R, Baloš S, Zlatanović DL, Sešek L, Pepelnjak T (2021) Characterisation of geometrical and physical properties of a stainless steel denture framework manufactured by single-point incremental forming. *J Mater Res Technol* 10:605–623. <https://doi.org/10.1016/j.jmrt.2020.12.014>
  242. Mishra S, Yazar KU, More AM, Kumar L, Lingam R, Reddy NV, Prakash O, Suwas S (2020) Elucidating the deformation modes in incremental sheet forming process: insights from crystallographic texture, microstructure and mechanical properties. *Mater Sci Eng A* 790:139311. <https://doi.org/10.1016/j.msea.2020.139311>
  243. Wei H, Hussain G, Heidarshenas B, Alkahtani M (2020) Post-forming mechanical properties of a polymer sheet processed by incremental sheet forming: insights into effects of plastic strain, and orientation and size of specimen. *Polymers-Basel*. 12. <https://doi.org/10.3390/polym12091870>
  244. Zhang P, Li J, Chen M (2020) Effect of different temperatures on the metallographic structure and tensile property of 2024–T4 alloy in integral heating single point incremental forming. *Microsc Res Technol* 83:920–927. <https://doi.org/10.1002/jemt.23485>
  245. Li Y, Chen X, Zhai W, Wang L, Li J, Guoqun Z (2018) Effects of process parameters on thickness thinning and mechanical properties of the formed parts in incremental sheet forming. *Int J Adv Manuf Technol* 98:3071–3080. <https://doi.org/10.1007/s00170-018-2469-9>
  246. Liu Z (2017) Friction stir incremental forming of AA7075-O sheets: investigation on process feasibility. *Procedia Eng* 207:783–788. <https://doi.org/10.1016/j.proeng.2017.10.829>
  247. Qiaoxin Z, Guohao L, Zhaobing L, Anguo Z, Xinhong X, Yongjie L (2018) Friction stir incremental forming of AA7075-O sheets: experimental investigations on performance evaluation of formed parts. *Rare Metal Mater Eng* 47:3659–3665. [https://doi.org/10.1016/S1875-5372\(19\)30014-1](https://doi.org/10.1016/S1875-5372(19)30014-1)
  248. Ilyas M, Hussain G, Rashid H, Alkahtani M (2020) Influence of forming parameters on the mechanical behavior of a thin aluminum sheet processed through single point incremental forming. *Metals-Basel* 10:1461. <https://doi.org/10.3390/met10111461>
  249. Hussain G, Ilyas M, Lemopi Isidore BB, Khan WA (2020) Mechanical properties and microstructure evolution in incremental forming of AA5754 and AA6061 aluminum alloys. *Trans Nonferrous Metal Soc* 30:51–64. [https://doi.org/10.1016/S1003-6326\(19\)65179-4](https://doi.org/10.1016/S1003-6326(19)65179-4)
  250. Wang H, Gu Y, Guo X, Wang H, Tao J, Xu Y (2018) Microstructure and mechanical properties of 2060–T8 Al–Li alloy after warm incremental forming. *J Mech Sci Technol* 32:4801–4812. <https://doi.org/10.1007/s12206-018-0927-9>
  251. Guo X, Guo X, Gu Y, Gu Y, Wang H, Wang H, Jin K, Jin K, Tao J, Tao J (2018) The Bauschinger effect and mechanical properties of AA5754 aluminum alloy in incremental forming process. *Int*

- J Adv Manuf Technol 94:1387–1396. <https://doi.org/10.1007/s00170-017-0965-y>
252. Xu R, Shi X, Xu D, Malhotra R, Cao J (2014) A preliminary study on the fatigue behavior of sheet metal parts formed with accumulative-double-sided incremental forming. *Manuf Lett* 2:8–11. <https://doi.org/10.1016/j.mfglet.2013.10.009>
253. Emmens WC, Hirt G, Tekkaya AE, van den Boogaard AH (2011) Formability in incremental sheet forming and cyclic stretch-bending. *Steel Res Int special*:513–518
254. Agrawa A, Ziegert J, Smith S, Woody B, Cao J (2012) Study of dimensional repeatability and fatigue life for deformation machining bending mode. *J Manuf Sci E- T ASME* 134
255. Nirala HK, Agrawal A (2021) Reprint of: Residual stress inclusion in the incrementally formed geometry using Fractal Geometry Based Incremental Toolpath (FGBIT). *J Mater Process Technol* 287:116623. <https://doi.org/10.1016/j.jmatprotec.2020.116623>

**Publisher's note** Springer Nature remains neutral with regard to jurisdictional claims in published maps and institutional affiliations.